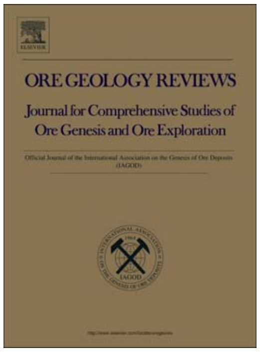

The role of black shales as a source of sulfur and semimetals in magmatic nickel-copper deposits: Example from the Partridge River Intrusion, Duluth Complex, Minnesota, USA

N. Samalens, S-J. Barnes, E.W. Sawyer

PII: S0169-1368(15)30107-4
DOI: doi: 10.1016/j.oregeorev.2016.09.030
Reference: OREGEO 1955

To appear in: *Ore Geology Reviews*

Received date: 6 October 2015
Revised date: 20 September 2016
Accepted date: 23 September 2016

Please cite this article as: Samalens, N., Barnes, S.-J., Sawyer, E.W., The role of black shales as a source of sulfur and semimetals in magmatic nickel-copper deposits: Example from the Partridge River Intrusion, Duluth Complex, Minnesota, USA, *Ore Geology Reviews* (2016), doi: 10.1016/j.oregeorev.2016.09.030

The role of black shales as a source of sulfur and semimetals in magmatic nickel-copper deposits: Example from the Partridge River Intrusion, Duluth Complex, Minnesota, USA.

Samalens N.*[1], Barnes S-J. [1], Sawyer E.W.[1]

[1] Université du Québec à Chicoutimi, 555 boulevard de l'Université, Saguenay, QC,

G7H 2B1, Canada

(*corresponding author e-mail: n.samalens@gmail.com)

Abstract

The basal unit of the Duluth Complex (Minnesota, USA) contains Ni-Cu sulfide deposits. The S in these is thought to be derived from a sulfide-rich black shale unit known as the Bedded Pyrrhotite Unit, a stratigraphic unit within the Virginia Formation host rocks. However, the mechanism of S transfer has not been clearly established. In order to understand how this transfer occurs we have undertaken petrography and whole rock geochemistry of the rocks from the contact aureole and the basal unit.

In the contact aureole, the Bedded Pyrrhotite Unit consists of a very fine-grained graphitic shales with thin beds of sulfides consisting of pyrrhotite with minor chalcopyrite (<1%). The basal unit contains numerous Bedded Pyrrhotite Unit xenoliths surrounded by norites. The Bedded Pyrrhotite Unit xenoliths are partially melted and the sulfide beds are disrupted. Leucosomes are present and these contain blebs of sulfides consisting of pyrrhotite, pentlandite, cubanite and chalcopyrite. In the mafic rocks surrounding the xenoliths small patches of sulfide-bearing leucosome are found. In addition to being rich in S the Bedded Pyrrhotite Unit is rich in As 38 ppm, Sb 4.1 ppm and Bi 0.6 ppm and Te 0.4 ppm and has high δ^{34}S values. The δ^{34}S, As/S, Bi/S and Sb/S decrease with distance from the xenoliths. Similarly, the Ni/S, Cu/S, Se/S and (platinum-group elements)/S ratios are higher in the mafic rocks and increase with distance from the xenoliths.

Our model proposes that droplets of sulfide melt derived from the Bedded Pyrrhotite Unit xenoliths were entrained in the anatectic silicate melt of the xenoliths and transferred to the mafic magma. The sulfide droplets equilibrated with the mafic magma. Those close to the xenoliths did not have the opportunity to react with a large quantity of magma, and hence their composition is similar to the sulfides of the Bedded Pyrrhotite Unit, i.e., rich in semimetals and poor in Ni, Cu and PGE. Farther away from the xenoliths, the sulfide droplets could have reacted with more magma, and the composition of these sulfides approach that of sulfides derived mainly from mafic magma.

Keywords. Duluth Complex; Proterozoic black shales; *in-situ* contamination; partial melting; diffusion; Ni deposits; magmatic sulfides.

Introduction

Much of the S in the world's magmatic Ni-Cu-platinum-group element (PGE) deposits is thought to be derived from external sources in the country rocks (Lesher et al., 1984; Ripley and Li, 2013). It is generally thought that S is derived from black shales (Thériault and Barnes, 1998; Lesher and Burnham, 2001). The world famous Noril'sk-Talnakh deposits may be an exception (Grinenko, 1985; Li et al., 2003). Sulfur is not the only element that could be derived from a black shale source. Black shales are enriched in As, Sb, Te and Bi by 1 to 3 orders of magnitude relative to Mid-Ocean Ridge Basalts, picrites and primitive mantle (Table 1). These elements are all chalcophile, and therefore contamination of a mafic magma with black shale could produce sulfide melts enriched in these elements compared to sulfide melts formed from mafic magmas. The semimetals may be important in concentrating PGEs within a Ni-Cu-PGE deposit because they are the anions required to form many platinum-group minerals (PGM).

A number of mechanisms for transfer of S from black shales to magma have been proposed: bulk melting of the country rock (Lesher and Burnham, 2001), transfer by gas or hydrothermal fluids (Baker et al., 2001; Ripley et al., 2007; Molnár et al., 2009; Benkó et al., 2015a, b), and transfer of sulfide droplets during partial melting of black shale xenoliths (Queffurus and Barnes, 2014). The Partridge River Intrusion of the Duluth Complex represents an ideal and well-documented intrusion for studying contamination processes because Ni-Cu sulfide deposits are found in the basal part of the intrusion close to the contact with S-rich black shales of the Virginia Formation (Mainwaring and Naldrett, 1977; Ripley, 1981; Andrews and Ripley, 1989; Thériault et al., 1997; Thériault and Barnes, 1998; Ripley et al., 2007; Severson and Hauck, 2008; Queffurus and Barnes, 2014; Robertson et al., 2015,Fig. 3), and detailed sampling is possible through numerous boreholes across the contact between the basal unit and the country rocks.

The sulfide-rich black shale unit is known as the Bedded Pyrrhotite Unit (Severson, 1994). Based on changes in $\delta^{34}S$ and S/Se values, the Bedded Pyrrhotite Unit has been identified as the source of the sulfur that contaminated the mafic magma (Zanko et al., 1994; Queffurus and Barnes, 2014). We have undertaken a petrographic, mineralogical and whole-rock geochemical study of the Bedded Pyrrhotite Unit country rocks, the Bedded Pyrrhotite Unit xenoliths and the enclosing mafic magma with the aim of investigating S and the behaviour of the semimetals during the interaction between the black shales and the mafic magma.

1. Geological context

The Duluth Complex is a Mesoproterozoic (1100 Ma) mafic complex located in Minnesota, USA. It consists of a number of mafic intrusions (Fig. 1) that are associated with the Midcontinent Rift System, and it is related to overlying the Keweenawan flood basalts (Severson and Hauck, 1997; Ojakangas et al., 2001; Miller and Severson, 2002). The country rocks range from Paleoproterozoic sedimentary rocks of the Animikie Group in the south to the Archean granite-greenstone in the north (Fig. 1).

Magmatic Ni-Cu deposits occur at the base of two of the intrusions, the Partridge River and the South Kawishiwi. Our study focused on the deposits of the Partridge River Intrusion (Fig. 1). The basal unit is composed of the following lithologies: norite, gabbronorite, troctolite and ultramafic rocks (Hauck et al., 1997; Thériault et al., 1997; Miller and Severson, 2002; Severson and Hauck, 2008). Norites correspond to the contaminated part of the magma and is localised in the vicinity of xenoliths in the basal part of the intrusion (Thériault et al., 1997; Queffurus and Barnes, 2014).

The deposits consist of disseminated to massive sulfides. The main minerals present are pyrrhotite, cubanite, chalcopyrite and pentlandite (Thériault and Barnes, 1998; Ripley, 2014). Massive sulfides are mainly found surrounding the country rocks xenoliths. Anastomosing veins and veinlets of massive sulfides are also found hosted by the gabbronorites, and in the country rocks close to the contact with the intrusion (Ripley and Alawi, 1986).

The country rocks of the Partridge River intrusion are Virginia Formation sedimentary rocks of the Animikie Group. The Virginia Formation is composed of carbonate, greywacke, pelite, black shale, and siltstone (Lucente and Morey, 1983). Away from the intrusion, the sedimentary rocks are essentially unmetamorphosed and the sulfide present is pyrite (Bonnichsen, 1972; Lucente and Morey, 1983, Fig. 2A; Queffurus and Barnes, 2014). However, close to the intrusion, the sedimentary rocks of the Virginia Formation have undergone contact metamorphism at temperatures hotter than 800°C, and formed diatexite migmatites close to the contact with the mafic magma (Labotka et al., 1981; Tracy and Frost, 1991; Sawyer, 2014).

One unit of particular interest is the Bedded Pyrrhotite Unit consisting of sulfide-rich black shales in the Virginia Formation and believed to have been deposited in restricted anoxic basins (Hauck et al., 1997). The Bedded Pyrrhotite Unit is mostly present close to the contact with the Duluth Complex (Severson and Hauck, 2008). This unit is approximately 200 m thick, but has a sporadic distribution. The basal unit of the Partridge River Intrusion (Unit I) contains numerous xenoliths of the Bedded Pyrrhotite Unit and the Virginia Formation (Ripley and Alawi, 1988; Thériault et al., 2000; Severson and Hauck, 2008; Queffurus and Barnes, 2014).

2. Methodology

Thirty-five samples were selected from diamond drill-hole cores that intersected the contact between the Virginia Formation and Partridge River Intrusion at the NorthMet, Mesaba, and Wetlegs deposits (Fig. 1 and Appendix A). Bedded Pyrrhotite Unit samples from the contact aureole come from boreholes AA-18 and A4-15. Xenoliths of the Bedded Pyrrhotite Unit, plus norites and gabbronorites, were collected from the NorthMet and Mesaba deposits (Fig. 1 and Appendix A). Data were combined with results from previous studies for a total database of 126 samples (Thériault et al., 1997; Thériault and Barnes, 1998; Thériault et al., 2000; Duchesne, 2004; Queffurus and Barnes, 2014).

Polished sections of each sample were obtained and petrographic observations were made, taking particular note of the sulfide mineralogy and textural changes between samples from the contact aureole, the xenoliths, and the norites.

Sulfur, Se, PGEs, and semimetals were determined at LabMaTer, Université du Québec à Chicoutimi (UQAC). Sulfur concentrations were determined by HORIBA EMIA-220V infrared and combustion S and C analyser using the method of Bédard et al., (2008). Platinum-group elements were determined by Ni-fire assay Te-co-precipitations and ICP-MS analysis and in addition, five samples were analysed by isotope dilution using the method of Savard et al., (2010). The semimetals in the black shales were determined using a new analytical protocol specially designed for black shales using an Agilent 7700X Series ICP-MS (Henrique-Pinto et al., 2016).

Major oxides and trace elements were determined at Activation Laboratories ltd (Actlabs), Ontario, Canada by Fusion ICP-MS (WRA42B). Sulfur isotopes were determined at the Environmental Isotope Laboratory (University of Waterloo, ON, Canada) using Elemental Analyzer-Isotope Ratio Mass Spectrometer (EA-IRMS) with V-CDT as internal standard.

Results for the certified reference materials are presented in appendix B.

3. Results

3.1 Petrography

Sulfide mineralogy and the form of the sulfides found within the contact aureole differ from those in the xenoliths. In samples of the Bedded Pyrrhotite Unit from the contact aureole partial melting occurred (Duchesne, 2004; Sawyer, 2014), and the rocks close to the contact with the intrusion are now diatexite migmatites with thin pyrrhotite beds (~0.5 to 3 mm thick) disrupted by a silicate anatectic melt network (Fig. 2A) that is now pseudomorphed by quartz, plagioclase and K-feldspar**.** The beds consist almost exclusively of pyrrhotite with rare (<1%) chalcopyrite intergrowths (Fig. 2B), but no pentlandite or cubanite.

In contrast, in the xenoliths the sulfide assemblage contains less pyrrhotite (~70 modal%), and more chalcopyrite, cubanite, and pentlandite (Fig. 2C). Angular shaped sulfide patches with low interfacial angles with the silicate phases, together with sulfide microveinlets that filled space between silicate grains, are observed at the margins of sulfide beds (Fig. 2D). There is also a variation in the proportion of sulfides within the xenoliths. In meter-sized xenoliths, the sulfide assemblages at the cores consists largely of pyrrhotite (~90 modal%), with some chalcopyrite and cubanite (~10 modal%), and little or no pentlandite (<1 modal%). The sulfide assemblage at the margins contain a large proportion of chalcopyrite and cubanite (up to 30 modal%), and some pentlandite (~5 modal%).

In some cases pyrrhotite-rich massive sulfides occur mixed with xenolith anatectic melt in a narrow zone (~5cm) at the edge of the Bedded Pyrrhotite Unit xenoliths (Fig. 2E). The sulfide assemblage consists of approximately equal amounts of pentlandite and chalcopyrite (~ 5 to 10 modal% of each), with the balance consisting of pyrrhotite.

The silicate portions of the Bedded Pyrrhotite Unit xenoliths have undergone partial melting. The mineralogical assemblage in the silicate portion of the Bedded Pyrrhotite Unit xenoliths is orthopyroxene + cordierite + biotite + plagioclase + melt +/- K-feldspar, graphite and ilmenite (Fig. 2F). Former melt pockets are composed of large (~500µm) K-feldspar and quartz grains with plagioclase, orthopyroxene, and less commonly cordierite inclusions. The melt pockets occur as films and interconnected networks, i.e., microleucosomes, in the xenoliths of the Bedded Pyrrhotite Unit. The xenolith mineralogical assemblage is consistent with those of the migmatites from the contact aureole that recorded temperatures hotter than 800°C (Sawyer, 2014).

Sulfide patches, which consist of an intergrowth of the sulfide minerals, commonly occur within the patches of former anatectic melt in the Bedded Pyrrhotite Unit xenoliths (Fig. 3A, B). The rounded shape of sulfide patches in anatectic melt contrasts with the angular shape of sulfides found in the matrix of the Bedded Pyrrhotite Unit xenoliths.

In addition, the zones (~5cm) around the xenoliths contains large amounts of anatectic melt (up to 50 modal%), and in some samples pyrrhotite-rich massive sulfides. These zones consist of xenolith anatectic melt mixed with the mafic magma (Fig. 3C, E). Relics of former anatectic melt consists of quartz-rich patches (~mm) and films (less than 100µm). Sulfide droplets (~50-200µm) are present in the anatectic melt (Fig. 3D, F).

4.2 Geochemistry

4.2.1 Chalcophile elements

The S content of the Bedded Pyrrhotite Unit from the contact aureole and the xenoliths ranges from ~ 0.5 to 10 % S. The $\delta^{34}S$ values vary from 16 to 20‰ in the contact aureole, and from 9 to 18‰ in the xenoliths (Fig. 4A). The massive sulfides contain 16 to 35 % S, and the $\delta^{34}S$ values range from 8 to 16‰, similar to the xenoliths. Most norites and gabbronorites are poorer in S, containing ~0.01 to 8.35% S; the δ^{34}S values are more depleted, ranging from 1.6 to ~15‰ (Fig.4A).

The metals are plotted versus S in order to examine whether they are hosted by sulfide minerals. Taking all the rock types together there is a broad correlation between the metals and S (Figs. 4 and 5). The mafic rocks are the most enriched in metals for a given S content, the xenoliths have an intermediate content, and the contact aureole rocks record the lowest metal contents (Figs. 4B, C, D and 5). The massive sulfides are richer in Ni and Co than the other rock types, and they lie along the extension of the trends for the mafic rocks. In contrast the massive sulfide samples contain more Cu than most, but not all, samples from other rock types.

Despite having similar S values, the Bedded Pyrrhotite Unit from the contact aureole has lower concentrations of chalcophile elements than the Bedded Pyrrhotite Unit xenoliths (Figs. 4B, C, D and 5). For example, the Cu content of rocks from the contact aureole is ~60 to 300 ppm, whereas the xenoliths contain ~150 to 4700 ppm. These observations are consistent with the petrographic observation that more chalcopyrite and pentlandite are observed in the Bedded Pyrrhotite Unit xenoliths than in the Bedded Pyrrhotite Unit rocks from the contact aureole.

Platinum-group elements and Ag also show broad correlations with S (Fig. 5A, B, C and D). The Bedded Pyrrhotite Unit rocks from the contact aureole have the lowest concentrations of platinum-group elements for a given S content, and the mafic rocks have the highest concentrations. The massive sulfides have greater Os, Ir, Ru and Rh concentrations than the other rocks types and the massive sulfides lie along the extension of the mafic rock trends (Ir and Rh shown in Fig. 5B, C). In contrast, the massive sulfides have contents similar in Pd, Pt, Au, and Ag to the S-rich xenoliths and mafic rocks (Pd and Ag shown in Fig. 5A, D).

The Bedded Pyrrhotite Unit rocks contain between 5 and 200 ppm As, similar to black shales averages from literature (Fig.6A and Table 1). The mafic rocks contain less As than the Bedded

Pyrrhotite Unit rocks, i.e., between 0.1 and 50 ppm, whereas the massive sulfides contains between 25 and 175 ppm, similar to the Bedded Pyrrhotite Unit. A broad correlation between As and S is shown for all the rock types. In general, the Bedded Pyrrhotite Unit rocks are richer in As than the mafic rocks for the same S content, and the Bedded Pyrrhotite Unit xenoliths appear to be particularly enriched in As.

The Bedded Pyrrhotite Unit rocks contain between 0.2 and ~10 ppm Sb, similar to black shale averages from the literature (Fig. 6B and Table 1). The mafic rocks record between ~0.05 and 4 ppm Sb, and the massive sulfides contain ~0.1 to 2 ppm Sb. There is no obvious correlation between Sb and S for the sample set as whole, but the norites show a moderate correlation.

The Bedded Pyrrhotite Unit rocks contain ~0.1 to 2 ppm Bi, and ~0.07 to 0.6 ppm Te, similar to black shale averages from literature (Fig. 6C, D, and Table 1). Mafic rocks contain ~0.1 to 5 ppm Bi and ~0.3 to 2 ppm Te. Mafic rocks contain higher Te contents for a given S content than the Bedded Pyrrhotite Unit rocks. The massive sulfides lie along the extension of the trend of the Bedded Pyrrhotite Unit.

4.2.2 Normalization to 100 % sulfides

In order to compare the composition of the sulfide component in each rock type the composition of the sulfide component has been calculated from the averages for the rocks containing more than 0.3 wt% S (Table 2). Sulfides from the Bedded Pyrrhotite Unit from the contact aureole contain the lowest Ni and Cu contents at 0.14 and 0.18 wt %, respectively, whereas the Bedded Pyrrhotite Unit xenolith sulfides have a higher Ni and Cu contents 0.75 and 1.7 wt %, respectively. The amount of Ni and Cu in the norite is greater than in the xenolith sulfides, and the gabbronorite contains the highest Ni and Cu contents at 4.5 and 13 wt % respectively. These calculated compositions are in agreement with the observations that the contact aureole does not contain pentlandite and only a little chalcopyrite, the xenolith sulfides contain some pentlandite and chalcopyrite, and the gabbronorite sulfides have the greatest concentrations of pentlandite and chalcopyrite.

Most of the other chalcophile elements (Co to Se on Fig. 7, Table 2) follow the same order of enrichment with the sulfides from the contact aureole having the lowest concentrations and the gabbronorite having the highest concentrations. In contrast, the elements from Bi to Mo show variable degrees of enrichment. Arsenic and Sb concentrations are the highest in the Bedded Pyrrhotite Unit xenoliths, whereas they are similar for the other rock types. Lead and Bi show similar concentrations in the xenoliths and the norites.

The overall shape of the mantle normalized patterns from all four rocks types is similar, with a steady increase from Co through the PGE to Ag (Fig. 7A) with Co/Ag of approximately 300 to 500. From Ag onwards the patterns tend to be approximately flat. Exceptions to these general trends are that the Bedded Pyrrhotite Unit from the contact aureole and the gabbronorite patterns have positive and negative Te anomalies, respectively.

The massive sulfides contain similar amounts of Co, Ni, Ir, Ru, and Rh to the norite sulfides, but they are depleted in most of the other chalcophile elements (Fig. 7B and Table 2). The mantle normalized concentrations increase from Co to Ag, but the pattern is not as steep as for the other sulfides, with a Co/Ag ratio of ~60 versus greater than 250 for the sulfides hosted by other rock types. The massive sulfides mantle normalized pattern show large negative Pt anomaly (Fig.7B).

4.2.3 Change in sulfide composition with distance from the Bedded Pyrrhotite Unit xenoliths

Queffurus and Barnes (2014) found that the sulfides close to the Bedded Pyrrhotite Unit xenoliths are poorer in Se than those close to the xenoliths. Thériault and Barnes (1997) found that there are more Sb- and As-bearing minerals present in the rocks close to the xenoliths. Our current more detailed sampling shows that As and Sb contents of norite and gabbronorite-hosted sulfides decrease with distance from the Bedded Pyrrhotite Unit xenoliths in the basal Unit I (Fig.

8A, B) whereas for most of the other elements the content increases (Pd and Ir shown in Fig.8C, D).

4. Discussion

5.1 Role of partial melting in contamination processes

Based on decreases in S/Se ratios and in δ^{34}S values, and the increase in (Pt+Pd)/S ratios from the Bedded Pyrrhotite Unit xenoliths into the norite and gabbronorite of the Unit I, Queffurus and Barnes (2014) argued that S was added to the mafic magma by partial melts of the Bedded Pyrrhotite Unit carrying sulfide droplets. Our petrographic observations support this model.

Metamorphosed Bedded Pyrrhotite Unit in the contact aureole, close to the contact with the intrusion, records temperatures of 800 to 870°C (Sawyer, 2014). Xenoliths of the Bedded Pyrrhotite Unit would have experienced even hotter temperatures as they were surrounded by mafic magma (~1100-1200°C; typical values for basaltic magma). Petrological features in the Bedded Pyrrhotite Unit xenoliths show pockets and pores of former anatectic melt pseudomorphed by large grains of K-feldspar and quartz that contain inclusions of orthopyroxene, plagioclase and cordierite. These features suggest that xenoliths of the Bedded Pyrrhotite Unit reached temperature of at least 800 to ~950°C in the granulite facies (White et al., 2003; Grant, 2009; Chu and Ague, 2013).

We interpret the rounded sulfide blebs found in the patches of former anatectic melt in the Bedded Pyrrhotite Unit xenoliths, and in the anatectic patches in the norite, as globules of a sulfide melt. We suggest that small droplets of sulfide melt were carried into the mafic magma by the silicate anatectic melt that was expelled from xenoliths of the Bedded Pyrrhotite Unit and in the process transferred S and semimetals to the mafic magma. Partial melting of sulfide minerals occurred in xenoliths of the Bedded Pyrrhotite Unit. The disrupted sulfide beds in the Bedded Pyrrhotite Unit xenoliths (Fig. 2D of this study; Fig. 2 of Queffurus and Barnes, 2014) reveal microstructures typical of sulfide partial melting, i.e., low interfacial angles between sulfide and silicate phases, and sulfide microveinlets that fill space between silicate grains (Frost et al., 2002; Tomkins et al., 2007). It might be thought that the melting temperature of pyrrhotite is too high (1190°C) for it to have melted. However, the presence of C, sulfosalts, and tellurides lowers the melting temperature of sulfides (Dasgupta et al., 2009, Tomkins et al., 2007), and thus the sedimentary sulfides could have melted.

5.2 Composition of sulfide droplets and massive sulfides

The composition of the sulfide droplets is expected to change from essentially sedimentary to igneous as they equilibrated with the mafic magma. Queffurus and Barnes (2014) modeled the changes in δ^{34}S, S/Se, and (Pt+Pd)/S using equations 5 and 8 of Lesher and Burnham (2001):

$$C_s = [(C_iR+C_{ss})D^{sul/sil}]/(R+D^{sul/sil})$$

$$I_s=\{I_iC_i[R/(1+R)]+I_{ss}C_{ss}[1/(1+R)]\}/\{C_i[R/(1+R)]+C_{ss}[1/(1+R)]\}$$

where C_s = concentration in the sulfide after equilibration; C_i=concentration of the element in the mafic magma; C_{ss}= concentration of the element in the sedimentary sulfides; R= ratio of silicate liquid to sulfide liquid; $D^{sul/sil}$ = partition coefficient between sulfide and silicate liquid; I_s= isotopic ratio in the sulfides after equilibration; I_i= isotopic ratio of mafic magma before contamination; and I_{ss}= isotopic ratio of the sedimentary sulfides.

A critical variable in these equations is the ratio of sulfide to silicate liquid. They found for the norites close to the xenoliths R-factors as low of 25 were required to model the sulfide composition, whereas for sulfides from the gabbronorite R-factors were up to 6000. We have applied this approach to our larger data sets (Table 3).

On the plot δ^{34}S vs. Cu in 100% sulfides, a progressive decrease of δ^{34}S occurs from the Bedded Pyrrhotite Unit xenoliths to the mafic magma with intermediate values for norites (Fig. 9A). Massive sulfides and norite-hosted sulfides close to xenoliths of the Bedded Pyrrhotite Unit plot at low R-factors (50), whereas most of gabbronorite-hosted sulfides require an R-factor greater than 500 (Fig. 9A).

Nickel, Cu, Co, and trace metals concentrations are highest in gabbronorite-hosted sulfides and lowest in sulfides from the Bedded Pyrrhotite Unit xenoliths; intermediate values occur in the norite-hosted sulfides (only Pd vs. Cu is shown in Fig. 9B). Thériault et al., (1997) proposed that the metal contents of norite and gabbronorite-hosted sulfides result from variations in the degree of magma contamination and R-factor. Modeling of sulfide composition after equilibration of Bedded Pyrrhotite Unit sulfides with the mafic magma is illustrated in figure 9B for Pd. The plot of Pd vs. Cu shows that massive sulfides and norite-hosted sulfides close to xenoliths of the Bedded Pyrrhotite Unit plot at R-factor values of 50 and 500 whereas most of the gabbronorite-hosted sulfides require higher R-factors (>500). Most of the other metals show similar results.

The results for the semimetals are more complex. Despite the fact that the Bedded Pyrrhotite Unit xenoliths are rich in Bi and Te, the sulfide component of the norite is richer in Bi and Te than the xenolith sulfides (Fig. 9C, D). Modeling shows that the concentrations of these elements rise in the sulfides as the R-factor increases, i.e., as the sulfide interacts with more mafic magma. This counter-intuitive result occurs because of the high partition coefficients for these elements into the sulfide liquid (Li and Audétat, 2015; Brenan, 2015). Although the mafic magma has low Bi and Te contents compared with the Bedded Pyrrhotite Unit xenoliths, the high partition coefficients of these elements into sulfides, combined with the high R-factor, results in the sulfide droplets from the Bedded Pyrrhotite Unit xenoliths collecting a large quantity of these elements (Fig. 9C, D).

In contrast, the Bedded Pyrrhotite Unit xenolith-hosted sulfides are richer in As and Sb than the norite or gabbronorite-hosted sulfides (Fig. 9E, F). Modeling of the sulfide compositions indicates that the concentrations of these elements decrease as the sedimentary sulfide interacts with the magma, but the observed sulfide compositions cover a wide range rather than a single trend (Fig. 9E, F). Possibly this wide range of results is due to the extreme sensitivity of the partition coefficients to fO_2 and temperature (Li and Audétat, 2015). At relatively cooler temperatures (900°C) in the xenolith, the partition coefficients would have been high (100-300), whereas at hotter temperatures (1100°C) in the mafic magma, the partition coefficients would have been lower (1-10). Consequently, the effect of higher R-factor in the mafic magma was offset by the lower partition coefficient in the mafic magma.

Thériault and Barnes (1998) show based on petrographic and geochemical observations that massive sulfides surrounding the xenoliths have undergone fractional crystallization. The massive sulfides in our current study are depleted in most of the chalcophile elements relative to Co, Ni, Ir, Ru, and Rh. This type of depletion is commonly observed in monosulfide-solid solution cumulates (Barnes et al., 1997). Given the position of the massive sulfides as narrow rims around the xenoliths; our interpretation is that they represent residual monosulfide-solid solution.

The sulfides hosted by the Bedded Pyrrhotite Unit from the contact aureole show similar chalcophile mantle-normalized patterns to the sulfides in the Bedded Pyrrhotite Unit xenoliths, but are depleted in all the chalcophile elements, except Se, relative to the sulfides in the xenoliths. It is possible that the contact aureole black shales initially had a slightly different composition to the xenoliths, but field observations suggest that they are the same unit. Another possibility is that the xenoliths have preferentially lost S and thus the recalculated sulfide compositions are too high. We do not think that this occurred because the xenolith and the contact aureole rocks contain on average similar amounts of S (~4%), and the xenolith sulfides are 3 to 10 times richer in most elements than the contact aureole sulfides, thus the xenoliths would have to have lost 66 % or more of their S. In other words, for elements such as Pd and Ni, which are strongly enriched, the xenoliths would have originally contained 24 to 40 % S. Therefore, we argue that the sulfides in the xenoliths have been enriched in chalcophile metals by diffusion of the elements from the mafic magma to the xenolith sulfides prior to the transfer of the sulfide droplets to the mafic magma. The reason for this diffusion was the chemical potential difference between the sulfide droplet in the anatectic melt in the xenolith and the chalcophile elements in the mafic magma.

5.3 Proposed model for S and semimetals contamination of the mafic magma

Based on petrological and geochemical observations, a synthesis model is proposed in Figure 10 to explain S and semimetals contamination of the mafic magma from xenoliths of the Bedded Pyrrhotite Unit:

1) Xenoliths of the Bedded Pyrrhotite Unit isolated in the gabbronorite magma of the basal unit, undergo partial melting at temperatures of ~900°C (Fig. 10A). Sulfide layers in the xenoliths undergo partial melting and sulfide droplets are incorporated in pockets of anatectic silicate melt. Simultaneously, diffusion of Ni, Cu, and trace metals may occur from the surrounding mafic magma into the xenoliths of the Bedded Pyrrhotite Unit.
2) Rounded droplets of sulfides in the anatectic silicate melt are transferred to the mafic magma (Fig. 10A). As a result, norites close to the xenoliths are enriched in semimetals. After dissolution of the silicate anatectic melt in the mafic magma, the entrained sulfide droplets interact and equilibrate with the mafic magma. This results in a minor metal enrichment of the sulfide droplets because of the low R-factor calculated for norite close to xenoliths of the Bedded Pyrrhotite Unit. Dissolution of sulfide droplets in the mafic magma leads to S contamination of the mafic magma as shown by Queffurus and Barnes

(2014), with progressive decrease of $\delta^{34}S$ values from the Bedded Pyrrhotite Unit xenoliths to the mafic magma.

3) As the degree of partial melting increases, connectivity between pores and pockets of melt is established and large volumes of silicate anatectic melt are segregated to the mafic magma leaving the xenoliths with residual bulk compositions (Fig. 10B). As a consequence, numerous sulfide droplets trapped in the silicate anatectic melt are also transferred to the mafic magma and norites close to the xenoliths record enrichment in semimetals. Accumulation of these sulfide droplets close to xenoliths could result in the formation of massive sulfide. These massive sulfides are poor in metals because there is no interaction between the sulfides and the mafic magma. Massive sulfides may undergo fractional crystallization and as a result they represent a monosulfide-solid solution cumulate, as was suggested by Thériault and Barnes (1998).
4) Movement of the magma, perhaps driven by a new injection of magma or by an earthquake in the partially molten system, allows bulk flow and hence transport of the sulfides away from the xenoliths, and this results in a larger-scale contamination of the mafic magma by S and semimetals (Fig. 10C). Hence, platinum-group minerals are found in sulfides from gabbronorites within the basal Unit I (McSwiggen, 1999; Severson and Hauck, 2003; Table 6a; Cervin, 2011). Enriched metal contents are recorded in sulfides away from the xenoliths, because of the interaction of the entrained sulfides with large volumes of magma, i.e., high R-factor.

5. Conclusions

Sulfur and semimetals contamination of the mafic magma occurs by the transfer of sulfide droplets in a mobile, silicate partial melt of the Bedded Pyrrhotite Unit xenoliths to the mafic magma. This conclusion is supported by:

1) Petrological observations of sulfide droplets trapped within former anatectic melt of the xenoliths of the Bedded Pyrrhotite Unit in the xenolith margins and surrounding the Bedded Pyrrhotite Unit xenoliths. We suggest that small droplets of sulfide melt were carried into the mafic magma by anatectic melt that was segregated from the Bedded Pyrrhotite Unit xenoliths.
2) Geochemical study which shows that a progressive decrease of $\delta^{34}S$ values from the Bedded Pyrrhotite Unit xenoliths to the mafic magma together with a progressive decrease of the semimetals content of norite- and gabbronorite-hosted sulfides occurs with distance from the Bedded Pyrrhotite Unit xenoliths in the basal Unit I.
3) Modeling of the composition of sulfides shows that the semimetals content of sulfides in the magma results from their equilibration after transfer to the mafic magma and depends on R-factor, i.e., interaction rate of sulfides with the mafic magma, and partition coefficients for these elements into the sulfide liquid.

In addition, petrographic and geochemical observations show that higher proportions of pentlandite and chalcopyrite occurs in the Bedded Pyrrhotite Unit xenoliths than in the Bedded Pyrrhotite Unit from the contact aureole, and that sulfides in the Bedded Pyrrhotite Unit from the contact aureole are depleted in Ni, Cu, and trace metals relative to the Bedded Pyrrhotite Unit xenolith-hosted sulfides. We propose that these elements diffused from the mafic magma to the Bedded Pyrrhotite Unit xenolith-hosted sulfides at temperatures in excess of 900°C.

Acknowledgments

This research was funded by the Natural Sciences and Engineering Research Council of Canada (NSERC) grant program and the Canada Research Chair in Magmatic Metallogeny. We thank Mark Severson for providing some samples of the Bedded Pyrrhotite Unit from the contact aureole. Sadia Medhi and Dany Savard from LabMaTer are thanked to help in carrying out analyses.We would like to thank Dr. Valentina Taranovic and an anonymous reviewer for helping us improve the clarity of our arguments. Dr. Franco Pirajno, Dr. Timothy Horscroft and Dr. Jeffrey Mauk are also thanked for their editorial handling and for inviting this paper.

References

Andrews, D., Ripley, E., 1989. Mass transfer and sulfur fixation in the contact aureole of the Duluth Complex, Dunka road Cu-Ni deposit, Minnesota. Can. Mineral. 27, 293-310.

Arevalo, Jr.R., McDonough, W.F., 2010. Chemical variations and regional diversity observed in MORB. Chem. Geol. 271, 70-85.

Baker, D.R., Barnes, S-J., Simon, G., Bernier, F., 2001. Fluid transport of sulfur and metals between sulfide melt and basaltic melt. Can. Mineral. 39, 537-546.

Barnes, S-J., Makovicky, E., Makovicky, M., Rose-Hansen, J., Karup-Moller, S., 1997. Partition coefficients for Ni, Cu, Pd, Pt, Rh, and Ir between monosulfide solid solution and sulfide liquid and the formation of compositionally zoned Ni – Cu sulfide bodies by fractional crystallization of sulfide liquid. Can. J. Earth Sci. 34, 366-374.

Barnes, S-J., 2016.Chalcophile elements. Encyclopedia of Geochemistry. Ed. W.M. White.In press.

Bédard, L.P., Savard, D., Barnes, S-J., 2008. Total sulfur concentration in geological reference materials by elemental infrared analyser. Geostand. Geoanal. Res. 32, 203-208.

Benkó, Z., Mogessie, A., Molnár, F., Krenn, K., Poulson, S.R., Hauck, S.A., Severson, M.J., Arehart, G.B., 2015a. Hydrothermal alteration and Cu–Ni–PGE mobilization in the charnockitic rocks of the footwall of the South Kawishiwi intrusion, Duluth Complex, USA. Ore Geol Rev. 67, 170-188.

Benkó, Z., Mogessie, A., Molnár, F., Severson, M.J., Hauck, S.A., Raič, S., 2015b. Partial Melting Processes and Cu-Ni-PGE Mineralization in the Footwall of the South Kawishiwi Intrusion at the Spruce Road Deposit, Duluth Complex, Minnesota.Econ.Geol. 110, 1269-1293.

Bonnichsen, W., 1972. Sulfide minerals in the Duluth Complex. In Sims, P. K., and Morey, G. W., eds., Geology of Minnesota: A centennial volume: Minn. Geol. Survey.pp. 388-393.

Brenan, J.M., 2015. Se–Te fractionation by sulfide–silicate melt partitioning: Implications for the composition of mantle-derived magmas and their melting residues. Earth Planet. Sci. Lett. 422, 45-57.

Cervin, D.O., 2011. Characterization of precious metal mineral occurrences in the NorthMet deposit of the Partridge River Intrusion, Duluth complex, Minnesota, USA: Unpublished. M.Sc. thesis, University of Minnesota, 155 p.

Chu, X., Ague, J.J., 2013. Phase equilibria for graphitic metapelite including solution of CO_2 in melt and cordierite: implications for dehydration, partial melting and graphite precipitation. J. Metamorph. Geol. 31, 843-862.

Dasgupta, R., Buono, A., Whelan, G., Walker, D., 2009. High-pressure melting relations in Fe–C–S systems: Implications for formation, evolution, and structure of metallic cores in planetary bodies. Geochim. Cosmochim. Acta. 73, 6678-6691.

Dionne-Foster, C., 2007. Géologie et indices de Ni-Cu-EGP de la zone Frontier dans la ceinture de Cape Smith, Nouveau Québec: Unpublished. M.Sc. thesis, Université du Québec à Chicoutimi, 320 p.

Duchesne, L., 2004. Fusion partielle et microstructures associées dans l'auréole de contact du complexe igné de Duluth, Minnesota: Unpublished. M.Sc. thesis, Université du Québec à Chicoutimi, 217 p.

Frost, B.R., Mavrogenes, J.A., Tomkins, A.G., 2002. Partial melting of sulfide or deposits during medium- and high-grade metamorphism. Can. Mineral.40, 1-18.

Grant, J.A., 2009. Thermocalc and experimental modeling of melting of pelite, Morton Pass, Wyoming. J. Metamorph. Geol. 27, 571-578.

Grinenko, L.N., 1985. Sources of sulfur of the nickeliferous and barren gabbro-dolerite intrusions of the northwest Siberian platform. Int Geol Rev. 28, 695-708.

Hauck, S.A., Severson, M.J., Zanko, L., Barnes, S.-J., Morton, P., Alminas, H., Foord, E.E., Dahlberg, E.H., 1997. An overview of the geology and oxide, sulfide, and platinum-group element mineralization along the western and northern contacts of the Duluth Complex. Geol Soc Am, special paper. 312, 137‑185.

Henrique-Pinto, R., Barnes, S-J., Savard, D., Mehdi, S., 2016. Quantification of metals and semimetals in carbon-rich rocks: A new sequential protocol including extraction from humic substances. Geostand. Geoanal. Res. In press. doi: 10.1111/j.1751-908X.2015.00340.x.

Hu, Z., Gao, S., 2008. Upper crustal abundances of trace elements: A revision and update. Chem. Geol. 253, 205-221.

Ketris, M.P., Yudovich, Y.E., 2009. Estimations of Clarkes for Carbonaceous biolithes: World averages for trace element contents in black shales and coals. Int J Coal Geol. 78, 135-148.

Kiseeva, E.S., Wood, B.J., 2013. A simple model for chalcophile element partitioning between sulfide and silicate liquids with geochemical applications. Earth Planet. Sci. Lett. 383, 68-81.

Labotka, T.C., Papike, J.J., Vaniman, D.T. 1981. Petrology of contact metamorphosed argillite from the Rove Formation, Gunflint Trail, Minnesota. Am. Mineral. 66, 70-86.

Lesher, C., Arndt, N., Groves, D., 1984. Genesis of komatiite-associated nickel sulfide deposits at Kambalda, Western Australia: A distal volcanic model. Sulfide deposits in mafic and ultramafic rocks, Institute of Mining and Metallurgy, London, 10 p.

Lesher, C.M., Burnham, O.M., 2001. Multicomponent elemental and isotopic mixing in Ni–Cu–(PGE) ores at Kambalda, western Australia. Can. Mineral. 39, 421-446.

Li, C., Chai, C., Li, X., Mao, X., 1998. Determination of Platinum-Group Elements and Gold in Two Russian Candidate Reference Materials SCHS-1 and SLg-1 by ICP-MS after Nickel Sulfide Fire Assay Preconcentration.Geostand.Newslett. 22, 195-197.

Li, C., Ripley, E.M., Naldrett, A.J., 2003. Compositional variation of olivine and sulfur isotopes in the Noril'sk and Talnakh intrusions, Siberia: Implications for ore-forming processes in dynamic magma conduits. Econ. Geol. 98, 69-86.

Li, Y., Audétat, A., 2012. Partitioning of V, Mn, Co, Ni, Cu, Zn, As, Mo, Ag, Sn, Sb, W, Au, Pb, and Bi between sulfide phases and hydrous basanite melt at upper mantle conditions. Earth Planet. Sci. Lett. 355, 327-340.

Li, Y., Audétat, A., 2015. Effects of temperature, silicate melt composition, and oxygen fugacity on the partitioning of V, Mn, Co, Ni, Cu, Zn, As, Mo, Ag, Sn, Sb, W, Au, Pb, and Bi between sulfide phases and silicate melt. Geochim. Cosmochim. Acta. 162, 25-45.

Liu, Y., Brenan, J., 2015. Partitioning of platinum-group elements (PGE) and chalcogens (Se, Te, As, Sb, Bi) between monosulfide-solid solution (MSS), intermediate solid solution (ISS) and sulfide liquid at controlled fO_2–fS_2 conditions. Geochim. Cosmochim. Acta. 159, 139-161.

Lucente, M.E., Morey, G.B., 1983. Stratigraphy and sedimentology of the Lower Proterozoic Virginia Formation, northern Minnesota. Minnesota Geological Survey, Report of Investigations RI-28, 28 p.

Lyubetskaya, T., Korenaga, J., 2007. Chemical composition of Earth's primitive mantle and its variance: 1. Method and results. J. Geophys. Res.: Solid Earth. 112, 1-21.

Mainwaring, P.R., Naldrett, A., 1977. Country-rock assimilation and the genesis of Cu-Ni sulfides in the Water Hen Intrusion, Duluth Complex, Minnesota.Econ. Geol. 72, 1269-1284.

McSwiggen, P.L., 1999. Platinum-palladium group minerals, gold, silver, and cobalt in the Minnamax copper-nickel sulfide deposit, Duluth Complex, northeastern Minnesota. Minnesota Geological Survey, Report of Investigations RI-54, 29 p.

Miller, J.D., Jr., and Severson, M.J., 2002.Geology of the Duluth Complex: geology and mineral potential of the Duluth Complex and related rocks of northeastern Minnesota: Minnesota Geological Survey, Report of Investigations RI-58, 207p.

Molnár, F., Arehart, G.B., Poulson, S., Hauck, S., 2009. Sulfur isotope constraints for a dynamic magmatic sulfide ore deposition model in the sill-like South Kawishiwi Intrusion of the Duluth Complex, Minnesota. Geol. Soc. America., Annual Meeting, Portland, OR. Abstr. Vol. 41, 25 p.

Ojakangas, R.W., Morey, G.B., Green, J.C., 2001. The Mesoproterozoic midcontinent rift system, Lake Superior Region, USA.Sediment. Geol. 141–142, 421-442.

Patten, C., Barnes, S-J., Mathez, E.A., Jenner, F.E., 2013. Partition coefficients of chalcophile elements between sulfide and silicate melts and the early crystallization history of sulfide liquid: LA-ICP-MS analysis of MORB sulfide droplets. Chem. Geol. 358, 170-188.

Petrov, L.L., Kornakov, Y.N., Korotaeva, Il.,Anchutina, E.A., Persikova, L.A., Susloparova, V.E., Fedorova, I.N., Shibanov, V.A., 2004. Multi-Element Reference Samples of Black Shale. Geostand. Geoanal. Res. 28, 89-102.

Queffurus, M., Barnes, S-J., 2014. Selenium and sulfur concentrations in country rocks from the Duluth Complex, Minnesota, USA: Implications for formation of the Cu-Ni-PGE sulfides. Econ. Geol. 109, 785-794.

Ripley, E.M., 1981. Sulfur isotopic studies of the Dunka road Cu-Ni deposit, Duluth Complex, Minnesota. Econ. Geol. 76, 610-620.

Ripley, E.M., Alawi, J.A., 1986. Sulfide mineralogy and chemical evolution of the Babbitt Cu-Ni deposit, Duluth Complex, Minnesota. Can. Mineral. 24, 347-368.

Ripley, E.M., Alawi, J.A., 1988. Petrogenesis of pelitic xenoliths at the Babbitt Cu-Ni deposit, Duluth Complex, Minnesota, U.S.A. Lithos. 21, 143-159.

Ripley, E.M., Taib, N.I., Chusi, L., Moore, C.H., 2007. Chemical and mineralogical heterogeneity in the basal zone of the Partridge River Intrusion: implications for the origin of Cu–Ni sulfide mineralization in the Duluth Complex, Midcontinent Rift System. Contrib. Mineral. Petrol. 154, 35-54.

Ripley, E.M., Li, C., 2013. Sulfide saturation in mafic magmas: Is external sulfur required for magmatic Ni-Cu-(PGE) ore genesis? Econ. Geol. 108, 45-58.

Ripley, E.M., 2014. Ni-Cu-PGE Mineralization in the Partridge River, South Kawishiwi, and Eagle Intrusions: A review of contrasting styles of sulfide-rich occurrences in the Midcontinent Rift System. Econ. Geol. 109, 309-324.

Robertson, J., Ripley, E.M., Barnes, S.J., Li, C., 2015. Sulfur liberation from country rocks and incorporation in mafic magmas. Econ. Geol. 110, 1111-1123.

Savard, D., Bédard, L.P., Barnes, S-J., 2009. Selenium Concentrations in Twenty-Six Geological Reference Materials: New Determinations and Proposed Values. Geostand. Geoanal. Res. 33, 249-259.

Savard, D., Barnes, S-J., Meisel, T., 2010. Comparison between Nickel-Sulfur Fire Assay Te Co-precipitation and Isotope Dilution with High-Pressure Asher Acid Digestion for the Determination of Platinum-Group Elements, Rhenium and Gold. Geostand. Geoanal. Res. 34, 281-291.

Sawyer, E.W., 2014. The inception and growth of leucosomes: microstructure at the start of melt segregation in migmatites. J. Metamorph. Geol. 7, 695-712.

Severson, M.J., 1994. Igneous stratigraphy of the South Kawishiwi intrusion, Duluth Complex, northeastern Minnesota: Duluth, University of Minnesota, Natural Resources Research Institute, Technical Report, NRRI/TR-93/34, 210 p.

Severson, M.J., Hauck, S.A., 1997. Igneous Stratigraphy and Mineralization in the Basal Portion of the Partridge River Intrusion, Duluth Complex, Allen Quadrangle, Minnesota: Duluth, Minnesota, University of Minnesota, Natural Resources Research Institute, Technical Report, NRRI/TR-97/19, 102 p.

Severson, M.J., Hauck, S.A., 2003. Platinum group elements (PGEs) and platinum group minerals (PGMs) in the Duluth Complex: Duluth, Minnesota, University of Minnesota, Natural Resources Research Institute, Technical Report, NRRI/TR-2003/37, 312 p.

Severson, M.J., Hauck, S.A., 2008. Finish Logging of Duluth Complex Drill Core (And a Reinterpretation of the Geology at the Mesaba (Babbitt) deposit): Duluth, University of Minnesota, Natural Resources Research Institute, Technical Report, NRRI/TR-2008/17, 68 p.

Thériault, R.D., Barnes, S-J., Severson, M.J., 1997. The influence of country-rock assimilation and silicate to sulfide ratios (R-factor) on the genesis of the Dunka Road Cu – Ni – platinum-group element deposit, Duluth Complex, Minnesota. Can. J. Earth Sci. 34, 375-389.

Thériault, R.D., Barnes, S-J., 1998. Compositional variations in Cu-Ni-PGE sulfides of the Dunka road deposit, Duluth Complex, Minnesota: The importance of combined assimilation and magmatic processes. Can. Mineral. 36, 869-886.

Thériault, R.D., Barnes, S-J., Severson, M.J., 2000. Origin of Cu-Ni-PGE Sulfide Mineralization in the Partridge River Intrusion, Duluth Complex, Minnesota. Econ. Geol. 95, 929-943.

Tomkins, A.G., Pattison, D.R.M., Frost, B.R., 2007. On the initiation of metamorphic sulfide anatexis. J. Petrol. 48, 511-535.

Tracy, R.J., Frost, B.R., 1991. Phase equilibria and thermobarometry of calcareous, ultramafic and mafic rocks, and iron formations. Rev. Mineral. Geochem. 26, 207-289.

Webb, P.C., Thompson, M., Potts, P.J., Bédard, L.P., 2006.GeoPT18 - An international proficiency test for analytical geochemistry laboratories - Report on round 18/Jan 2006 (Quartz diorite, KPT-1). International Association of Geoanalysts, Report, 32p.

White, R.W., Powell, R., Clarke, G.L., 2003. Prograde metamorphic assemblage evolution during partial melting of metasedimentary rocks at low pressures: Migmatites from Mt Stafford, Central Australia. J. Petrol. 44, 1937-1960.

Whitney, D.L., Evans, B.W., 2010. Abbreviations for names of rock-forming minerals. Am. Mineral. 95, 185-187.

Zanko, L.M., Severson, M.J., Ripley, E.M., 1994. Geology and mineralization of the Serpentine copper-nickel deposit, Duluth Complex, Minnesota: Duluth, Minnesota, University of Minnesota, Natural Resources Research Institute, Technical Report, NRRI/TR-93/52, 90 p.

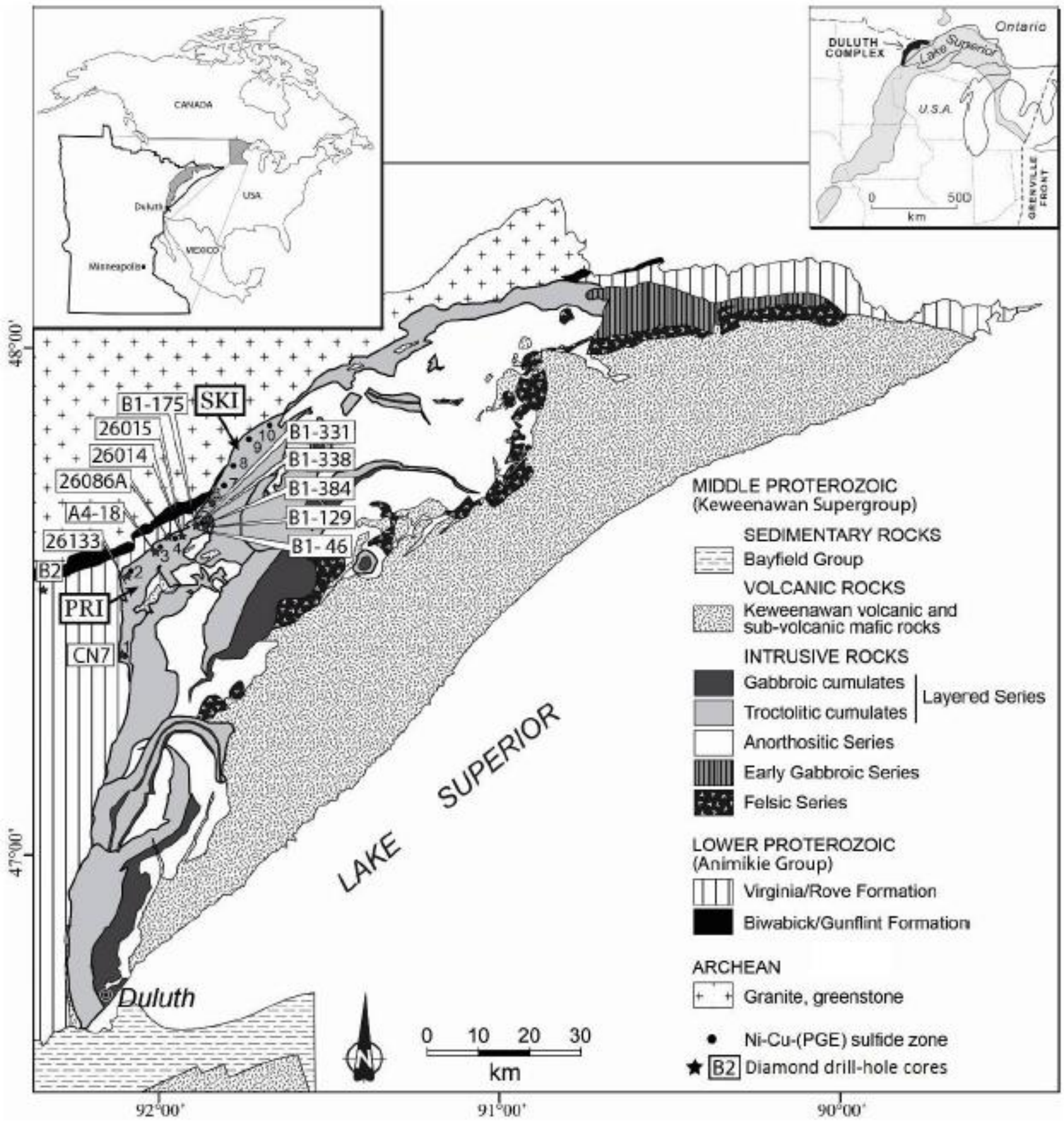
CANADA
USA
MEXICO
Duluth
Minneapolis
Ontario
DULUTH COMPLEX
Lake Superior
U.S.A.
0
500
km
GRENVILLE FRONT
48°00'
47°00'
92°00'
91°00'
90°00'
B1-175
SKI
26015
26014
26086A
A4-18
26133
B2
PRI
CN7
B1-331
B1-338
B1-384
B1-129
B1- 46
1
2
3
4
7
8
9
10
LAKE SUPERIOR
Duluth
N
0
10
20
30
km
MIDDLE PROTEROZOIC
(Keweenawan Supergroup)
SEDIMENTARY ROCKS
Bayfield Group
VOLCANIC ROCKS
Keweenawan volcanic and sub-volcanic mafic rocks
INTRUSIVE ROCKS
Gabbroic cumulates
Troctolitic cumulates
Layered Series
Anorthositic Series
Early Gabbroic Series
Felsic Series
LOWER PROTEROZOIC
(Animikie Group)
Virginia/Rove Formation
Biwabick/Gunflint Formation
ARCHEAN
Granite, greenstone
Ni-Cu-(PGE) sulfide zone
B2 Diamond drill-hole cores

Figure 1

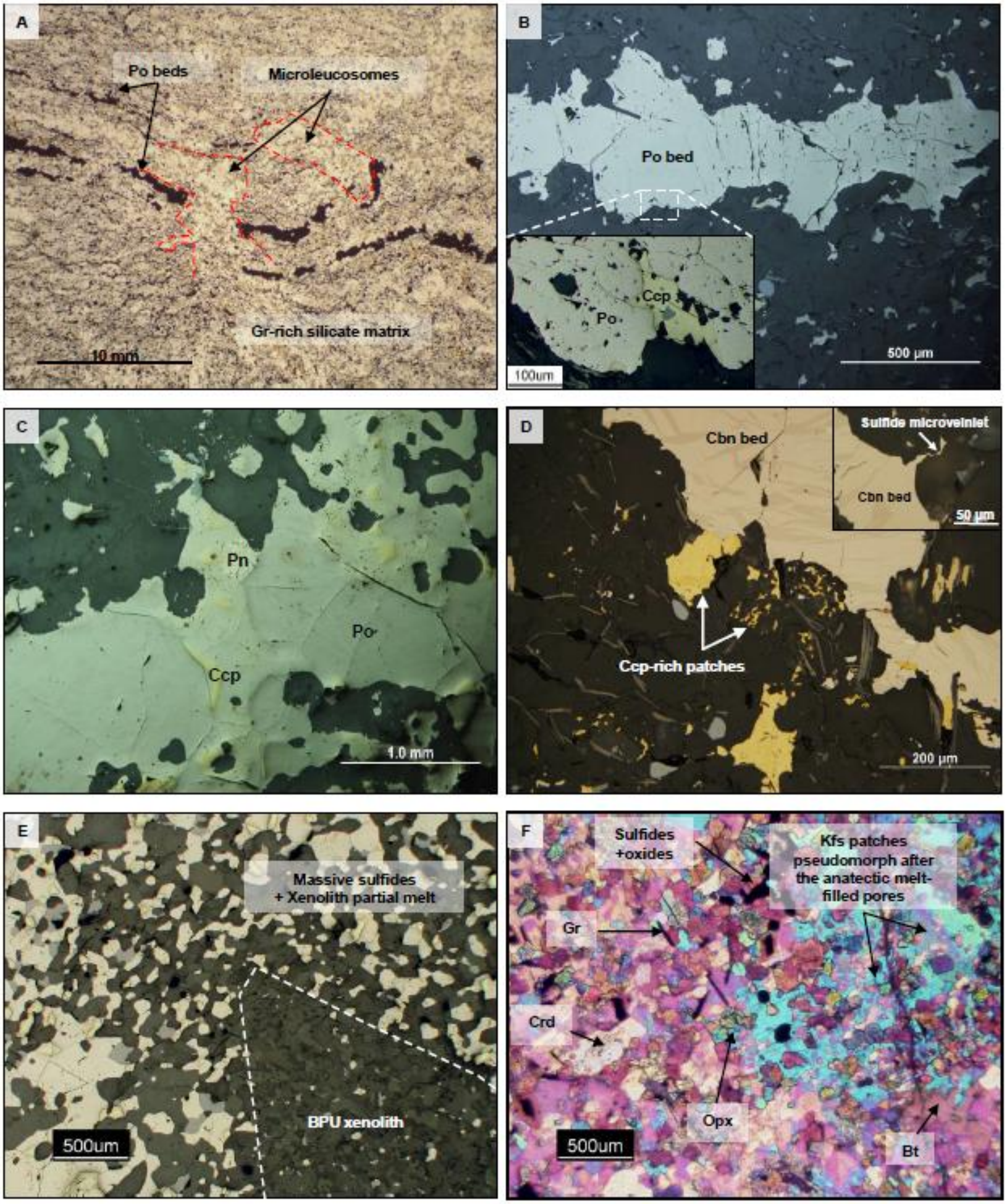
A
Po beds
Microleucosomes
Gr-rich silicate matrix
10 mm
B
Po bed
Po
Ccp
100um
500 µm
C
Pn
Po
Ccp
1.0 mm
D
Cbn bed
Sulfide microveinlet
Cbn bed
50 µm
Ccp-rich patches
200 µm
E
Massive sulfides
+ Xenolith partial melt
BPU xenolith
500um
F
Sulfides
+oxides
Kfs patches
pseudomorph after
the anatectic melt-
filled pores
Gr
Crd
Opx
Bt
500um

Figure 2

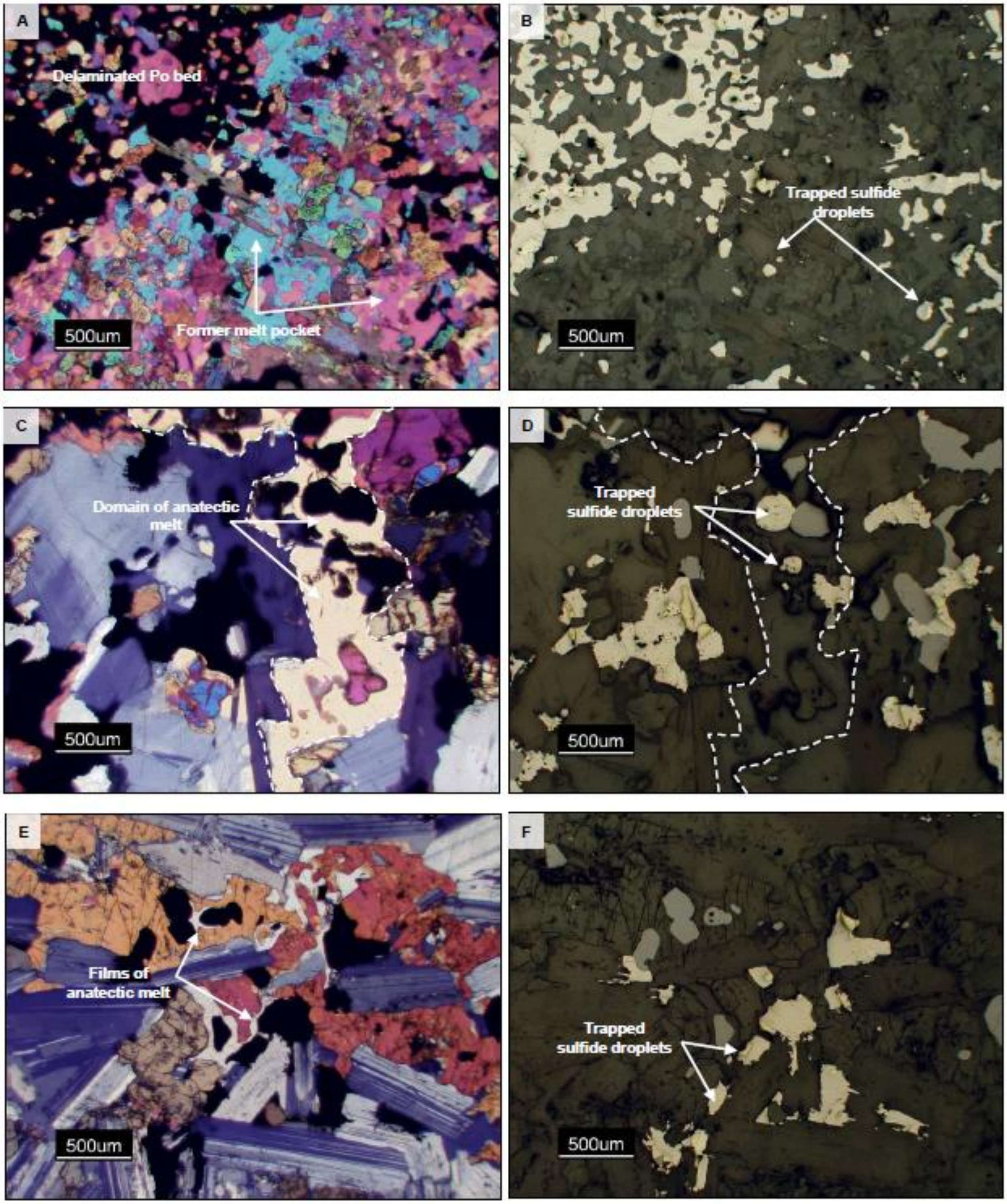
A
Delaminated Po bed
Former melt pocket
500um
B
Trapped sulfide droplets
500um
C
Domain of anatectic melt
500um
D
Trapped sulfide droplets
500um
E
Films of anatectic melt
500um
F
Trapped sulfide droplets
500um

Figure 3

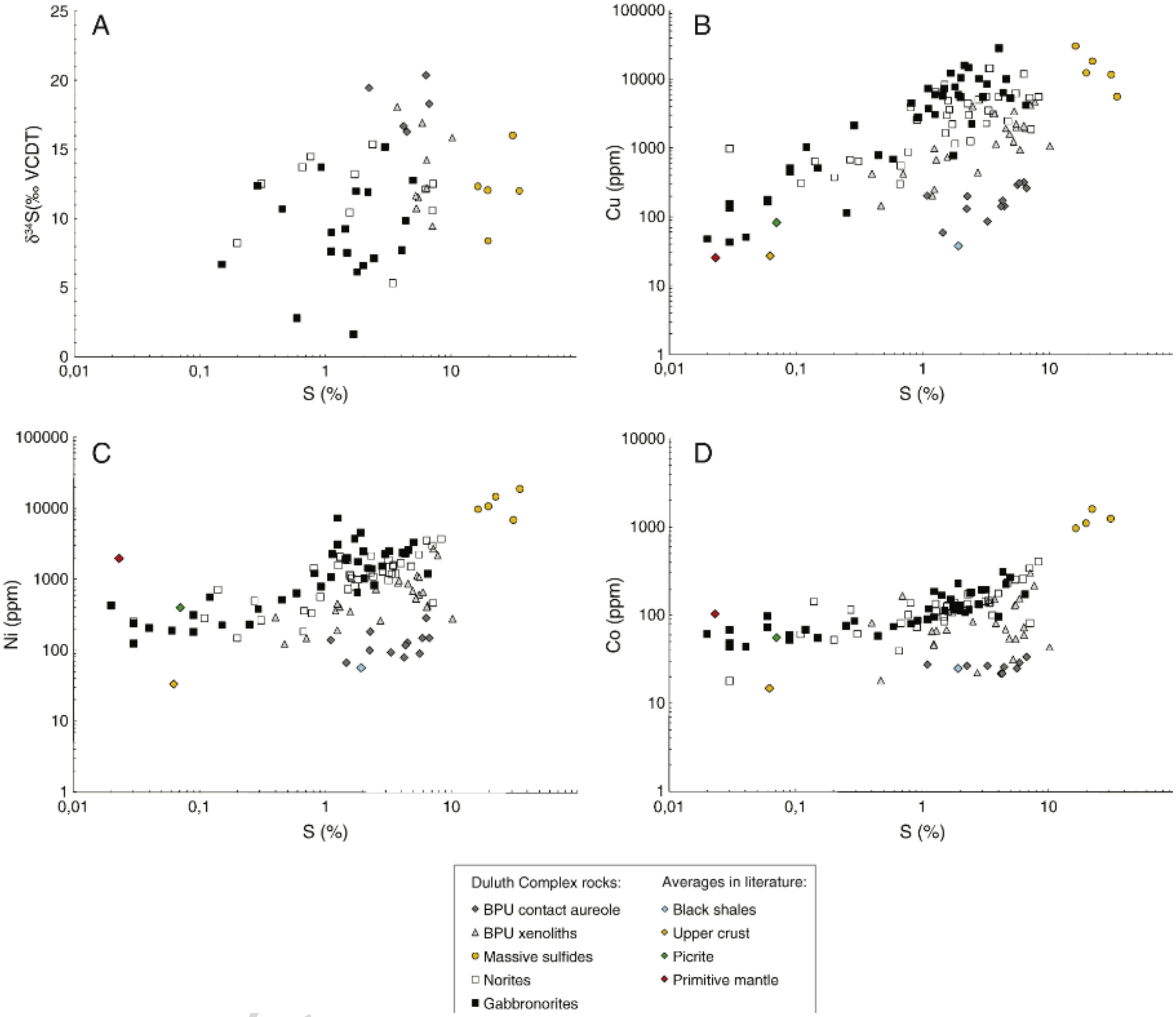
A
δ34S(‰ VCDT)
S (%)
B
Cu (ppm)
S (%)
C
Ni (ppm)
S (%)
D
Co (ppm)
S (%)
Duluth Complex rocks:
◆ BPU contact aureole
△ BPU xenoliths
● Massive sulfides
□ Norites
■ Gabbronorites
Averages in literature:
◆ Black shales
◆ Upper crust
◆ Picrite
◆ Primitive mantle

Figure 4

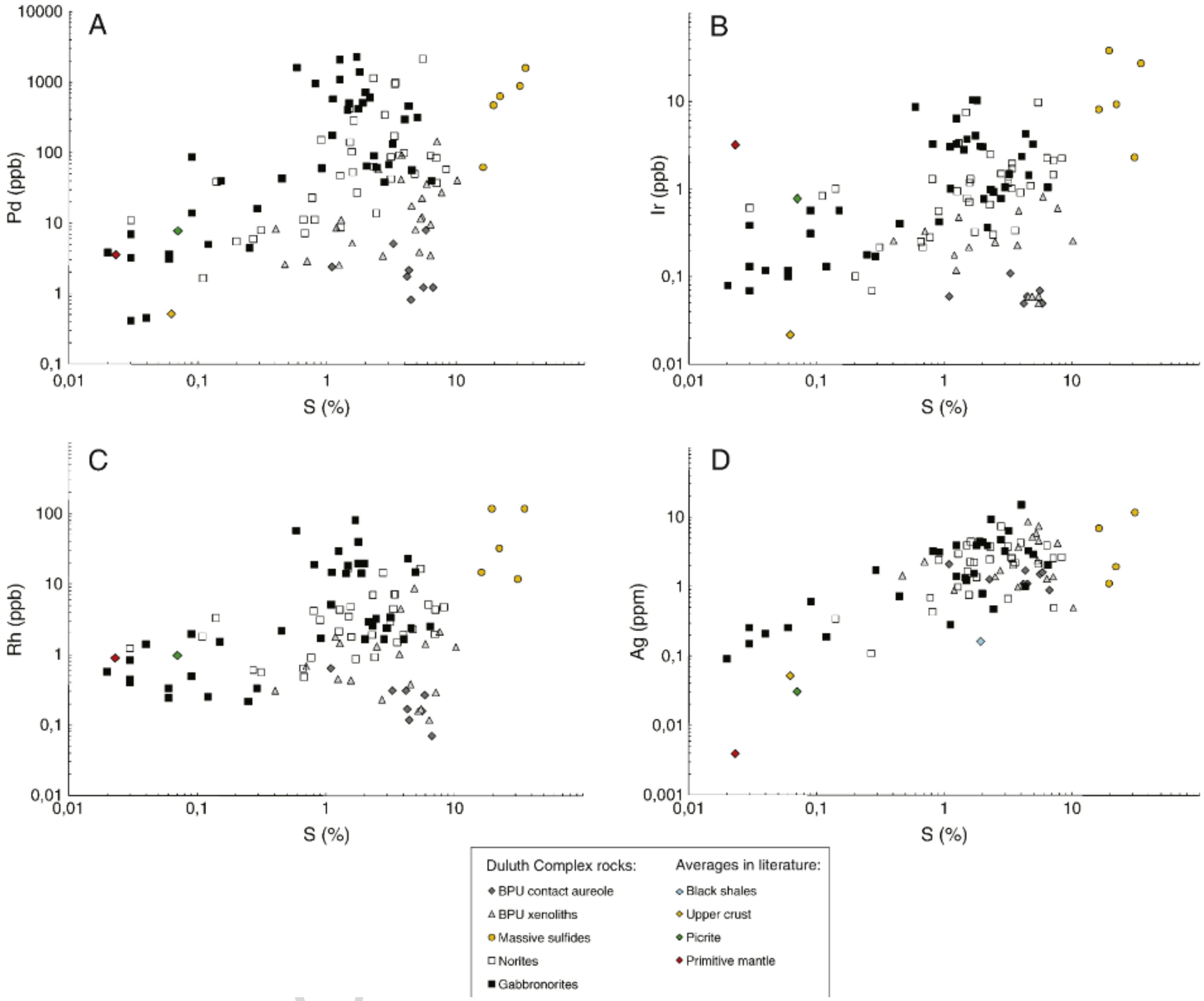
A
Pd (ppb)
10000
1000
100
10
1
0,1
S (%)
0,01
0,1
1
10
B
Ir (ppb)
10
1
0,1
0,01
S (%)
C
Rh (ppb)
100
10
1
0,1
0,01
S (%)
D
Ag (ppm)
10
1
0,1
0,01
0,001
S (%)
Duluth Complex rocks:
◆ BPU contact aureole
△ BPU xenoliths
● Massive sulfides
□ Norites
■ Gabbronorites
Averages in literature:
◆ Black shales
◆ Upper crust
◆ Picrite
◆ Primitive mantle

Figure 5

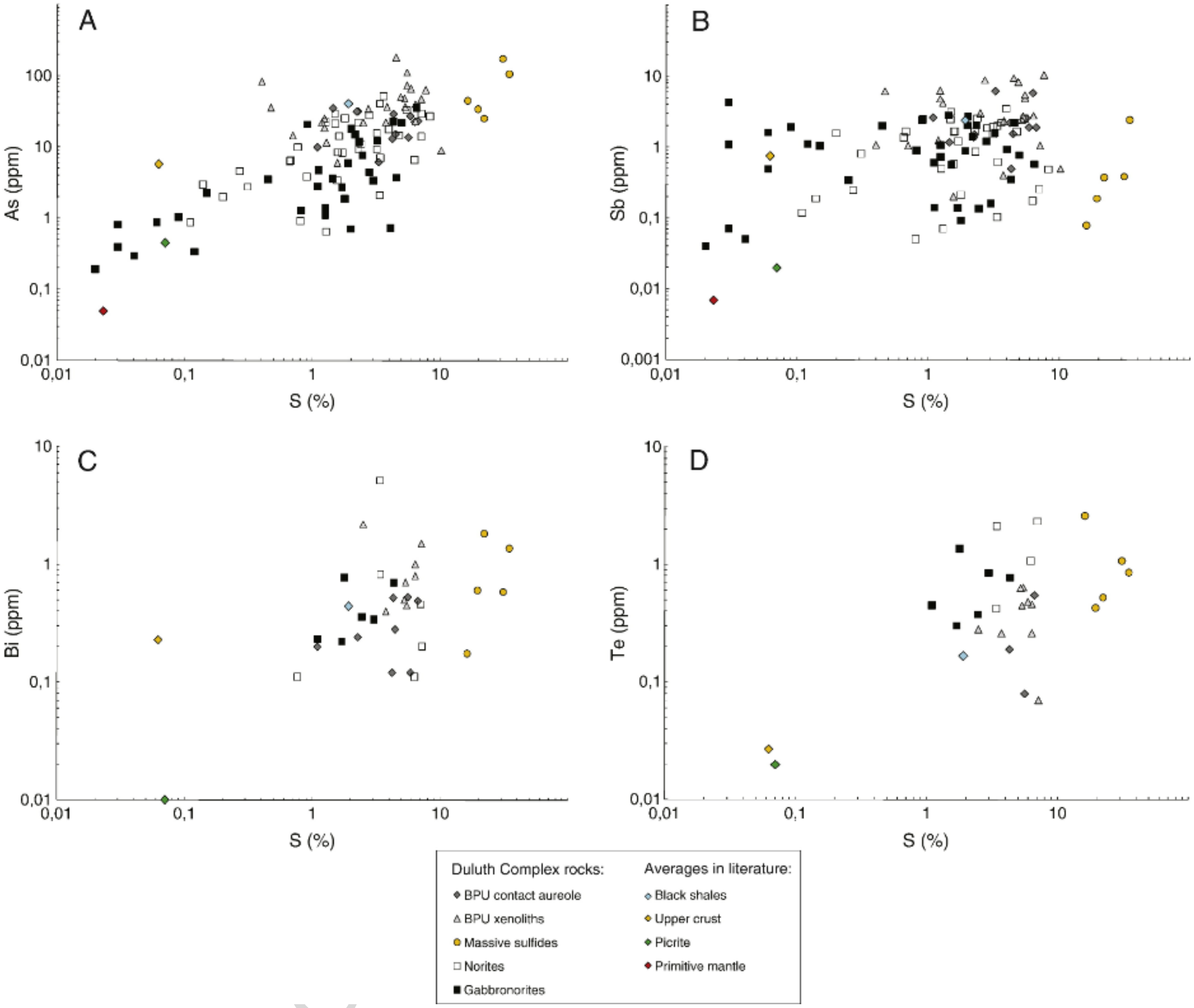
A
As (ppm)
100
10
1
0,1
0,01
0,01
0,1
1
10
S (%)
B
Sb (ppm)
10
1
0,1
0,01
0,001
0,01
0,1
1
10
S (%)
C
Bi (ppm)
10
1
0,1
0,01
0,01
0,1
1
10
S (%)
D
Te (ppm)
10
1
0,1
0,01
0,01
0,1
1
10
S (%)
Duluth Complex rocks:
BPU contact aureole
BPU xenoliths
Massive sulfides
Norites
Gabbronorites
Averages in literature:
Black shales
Upper crust
Picrite
Primitive mantle

Figure 6

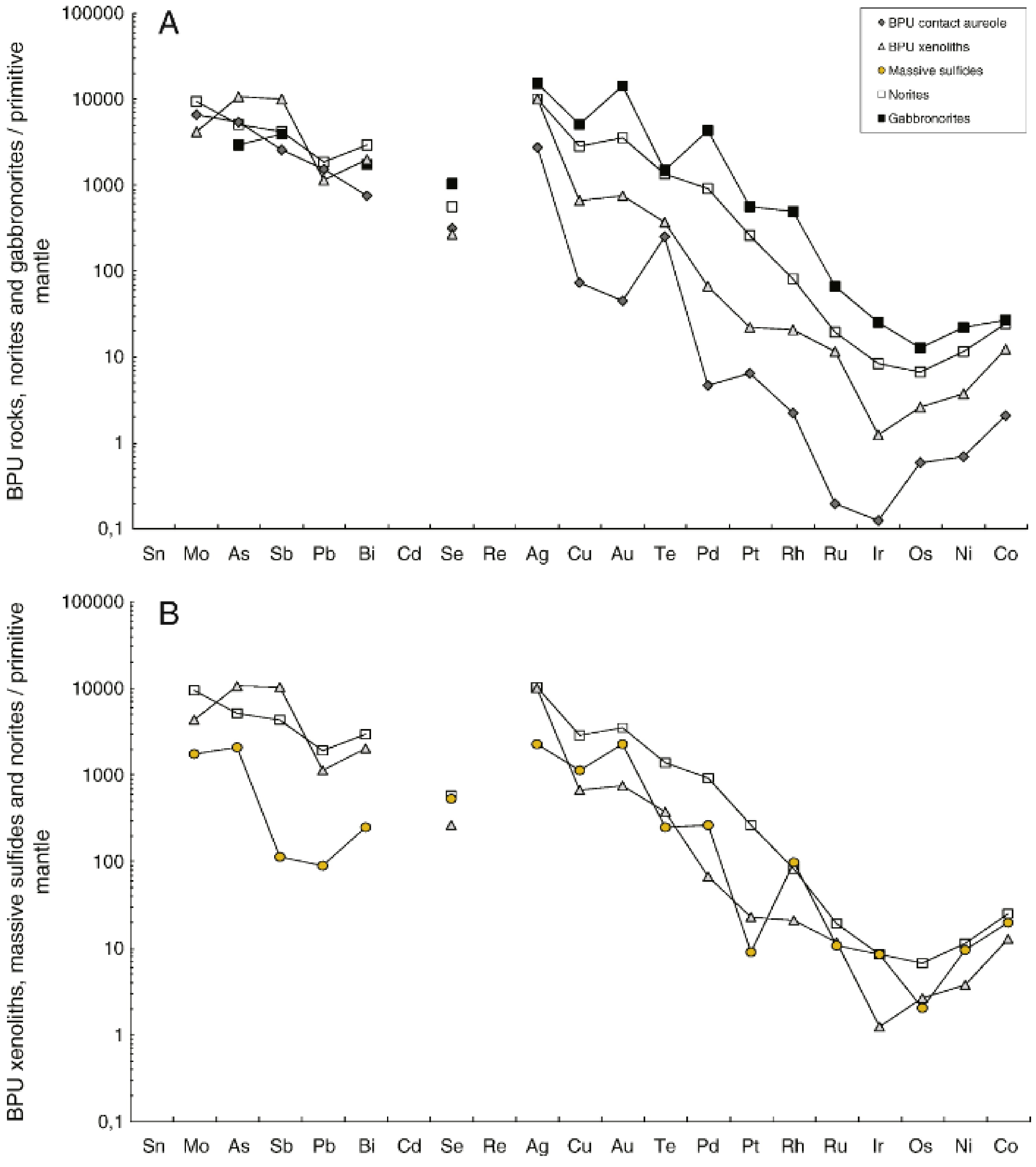
A
BPU rocks, norites and gabbronorites / primitive mantle
100000
10000
1000
100
10
1
0,1
◆ BPU contact aureole
△ BPU xenoliths
● Massive sulfides
□ Norites
■ Gabbronorites
Sn
Mo
As
Sb
Pb
Bi
Cd
Se
Re
Ag
Cu
Au
Te
Pd
Pt
Rh
Ru
Ir
Os
Ni
Co
B
BPU xenoliths, massive sulfides and norites / primitive mantle
100000
10000
1000
100
10
1
0,1
Sn
Mo
As
Sb
Pb
Bi
Cd
Se
Re
Ag
Cu
Au
Te
Pd
Pt
Rh
Ru
Ir
Os
Ni
Co

Figure 7

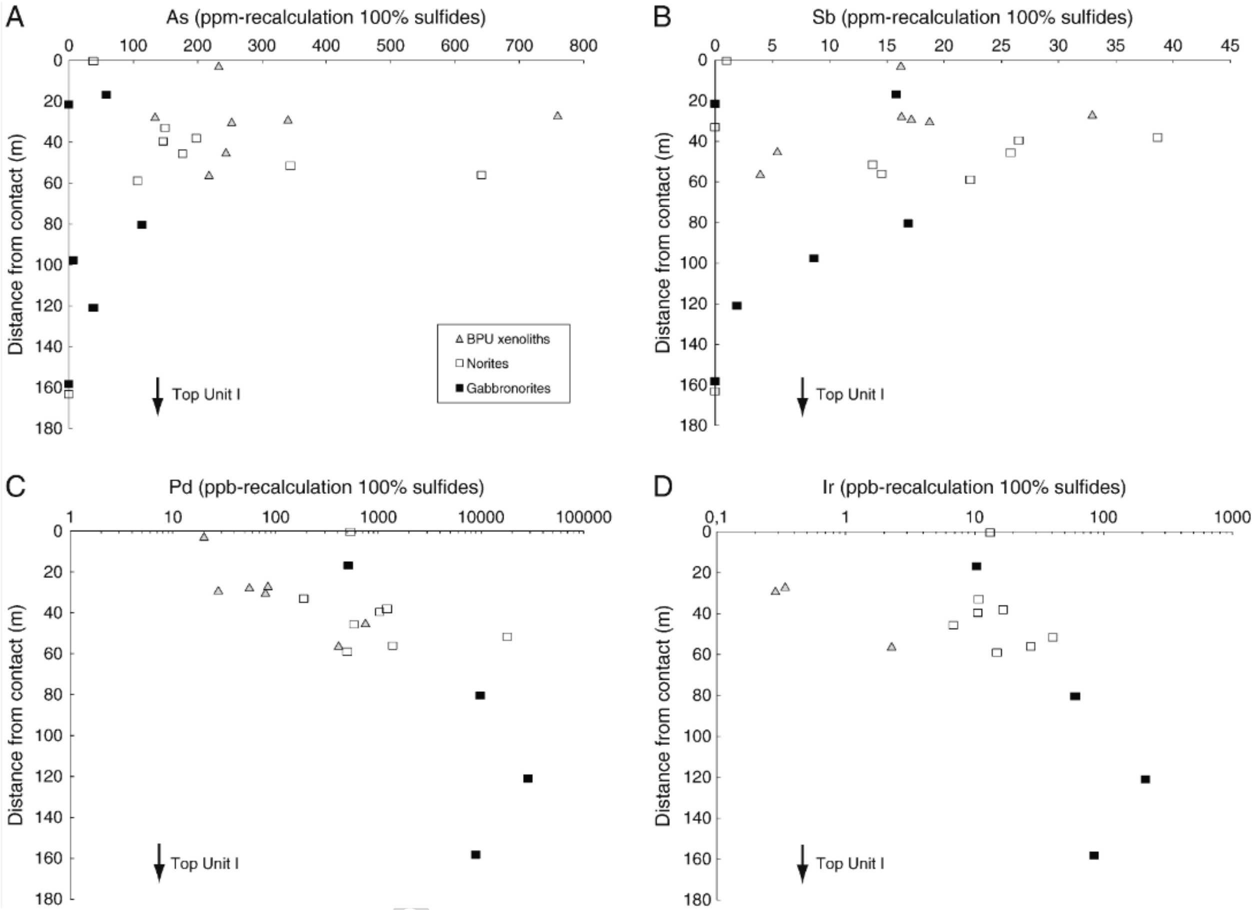
A
As (ppm-recalculation 100% sulfides)
0
100
200
300
400
500
600
700
800
Distance from contact (m)
0
20
40
60
80
100
120
140
160
180
Top Unit I
△ BPU xenoliths
□ Norites
■ Gabbronorites
B
Sb (ppm-recalculation 100% sulfides)
0
5
10
15
20
25
30
35
40
45
Distance from contact (m)
Top Unit I
C
Pd (ppb-recalculation 100% sulfides)
1
10
100
1000
10000
100000
Distance from contact (m)
Top Unit I
D
Ir (ppb-recalculation 100% sulfides)
0,1
1
10
100
1000
Distance from contact (m)
Top Unit I

Figure 8

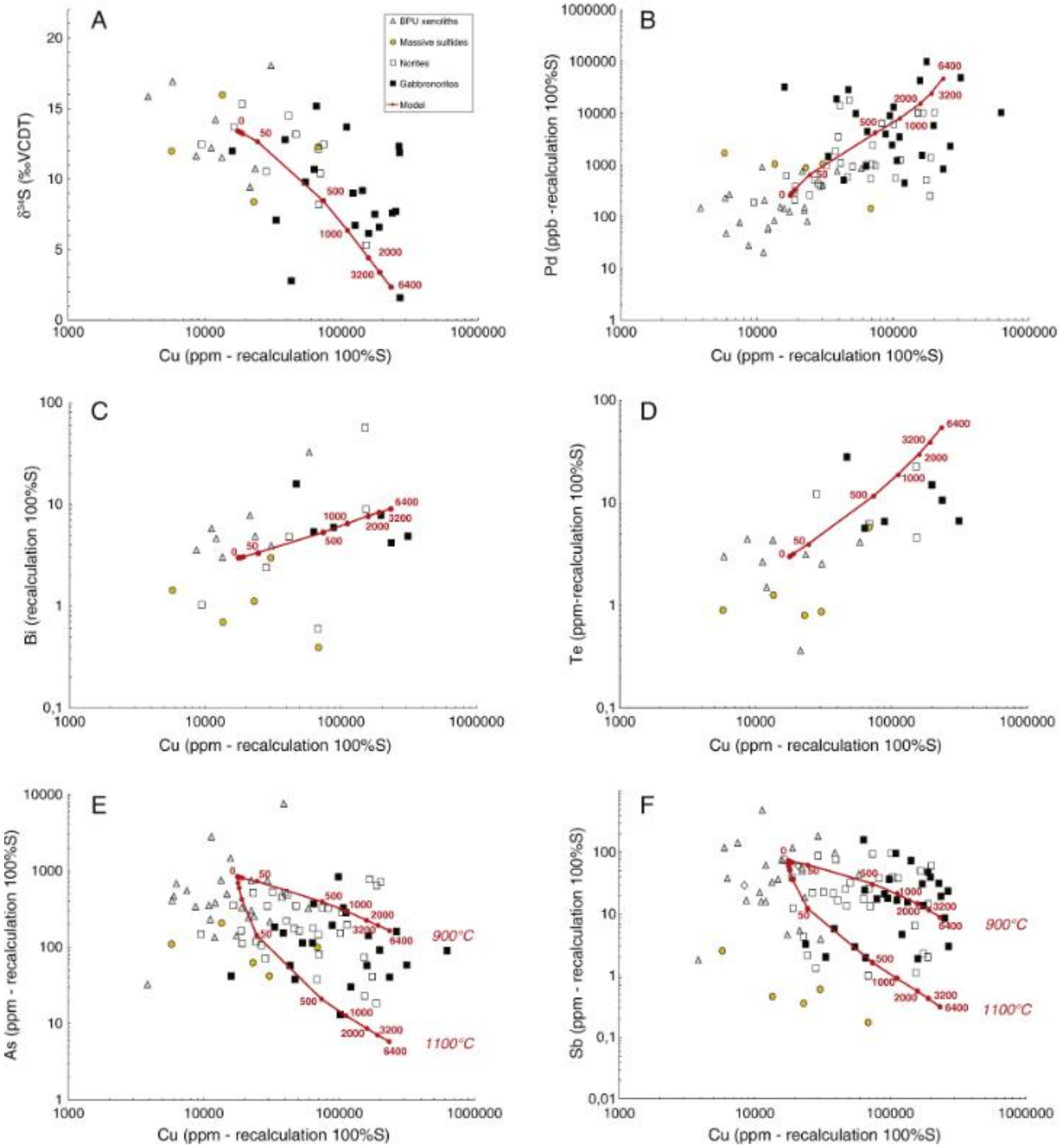
A
BPU xenoliths
Massive sulfides
Norites
Gabbronorites
Model
$\delta^{34}S$ (‰VCDT)
0
5
10
15
20
0
50
500
1000
2000
3200
6400
Cu (ppm - recalculation 100%S)
1000
10000
100000
1000000
B
Pd (ppb -recalculation 100%S)
1
10
100
1000
10000
100000
1000000
0
50
500
1000
2000
3200
6400
Cu (ppm - recalculation 100%S)
C
Bi (recalculation 100%S)
0,1
1
10
100
0
50
500
1000
2000
3200
6400
Cu (ppm - recalculation 100%S)
D
Te (ppm-recalculation 100%S)
0,1
1
10
100
0
50
500
1000
2000
3200
6400
Cu (ppm - recalculation 100%S)
E
As (ppm - recalculation 100%S)
1
10
100
1000
10000
0
50
500
1000
2000
3200
6400
900°C
1100°C
Cu (ppm - recalculation 100%S)
F
Sb (ppm - recalculation 100%S)
0,01
0,1
1
10
100
0
50
500
1000
2000
3200
6400
900°C
1100°C
Cu (ppm - recalculation 100%S)

Figure 9

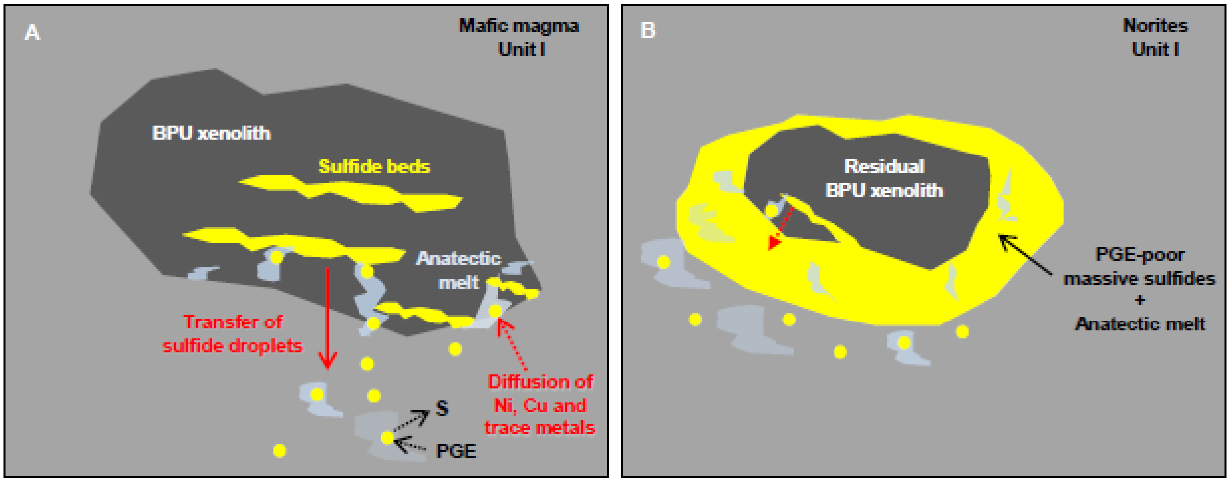

A) Xenolith partial melting

B) Increase of partial melting degree

C) Magma disturbance

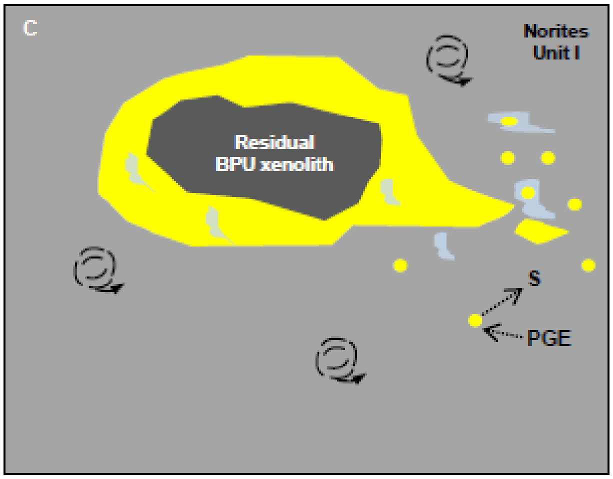

Figure 10

Fig. 1. Geological and location map of the Duluth Complex (modified from Queffurus and Barnes, 2014; Ojakangas et al., 2001; Miller et al., 2002). The right inset shows position of the Duluth Complex in the Midcontinent Rift System.

Abbreviations: PRI = Partridge River intrusion, SKI = South Kawishiwi intrusion. Ni-Cu-PGE deposits : 1, Water Hen; 2, Wyman Creek; 3, Wetlegs; 4, NorthMet (Dunka Road); 5, Mesaba (Babbitt); 6, Serpentine; 7, Dunka Pit; 8, Birch Lake; 9, Nokomis; 10. Diamond drill-hole cores are indicated by stars.

Fig. 2. Photomicrographs of Bedded Pyrrhotite Unit (BPU) Sulfides and silicates textures from the contact aureole and inside the intrusion.

A) Sulfide beds crosscut by anatectic melt in partially molten BPU from the contact aureole. B) Pyrrhotite bed in BPU metamorphosed from the contact aureole. Inset shows details for chalcopyrite grain in pyrrhotite bed. Notice that pentlandite and cubanite are absent of BPU country rocks. C) Sulfide bed in BPU xenolith within the intrusion. D) Delaminated sulfide bed in BPU xenolith. Chalcopyrite-rich patches close to the sulfide bed and sulfide microveinlets. Low angle interfaces occurs between sulfides and silicates. E) Massive sulfides surrounding BPU xenolith within the intrusion. F) Silicate mineralogical assemblage in a partially melted BPU xenolith. Quartz plate is added to better identify the inclusions of former anatectic melt.

Abbreviations (Whitney and Evans, 2010): Silicates: Bt = Biotite; Opx = Orthopyroxene; Crd = Cordierite; Pl = Plagioclase; Kfs = K-Feldspar; Qtz = Quartz. Sulfides: Ccp = Chalcopyrite; Cbn = Cubanite; Po = Pyrrhotite; Pn = Pentlandite. Gr = Graphite.

Fig. 3. Photomicrographs of partial melting textures of Bedded Pyrrhotite Unit (BPU) xenoliths and surrounding zones.

A) Detached pyrrhotite bed in BPU xenoliths in contact with melt filled space between the grains in BPU xenolith. Quartz plate is added to better show anatectic melt pockets. B) Sulfide droplets in pockets of anatectic melt pockets in same area of the photomicrograph A). C) Anatectic melt patches with trapped sulfide droplets in the anatectic melt-rich zone surrounding BPU xenolith. D) Rounded sulfide droplets trapped in xenolith anatectic melt patches from same area as the photomicrograph C). E) Films of anatectic melt that contained sulfide droplets in zones surrounding the BPU xenolith. F) Details of sulfide droplets trapped in small pockets of anatectic melt, same area than photomicrograph E).

Abbreviation: BPU = Bedded Pyrrhotite Unit.

Fig. 4. Plots of (A) $\delta_{34}S$ isotopic ratio, (B) Ni, (C) Cu and (D) Co vs. S.

Isotopic ratio $\delta_{34}S$ of mantle is comprised between 0 to 1‰. Averages of black shales, upper crust, picrites, and primitive mantle are shown for reference (Dionne-Foster, 2007; Lyubetskaya and Korenaga, 2007; Hu and Gao, 2008; Henrique-Pinto et al., 2016). Abbreviation: BPU = Bedded Pyrrhotite Unit.

Fig. 5. Trace metals (A) Pd, (B) Ir, (C) Rh and (D) Ag vs. S for all rocks.

Averages of black shales, upper crust, picrites, and primitive mantle are shown for reference (Dionne-Foster, 2007; Lyubetskaya and Korenaga, 2007; Hu and Gao, 2008; Henrique-Pinto et al., 2016). Abbreviation: BPU = Bedded Pyrrhotite Unit.

Fig. 6. Semimetals (A) As, (B) Sb, (C) Bi and (D) Te vs. S for all rocks.

Averages of black shales, upper crust, picrites, and primitive mantle are shown for reference (Dionne-Foster, 2007; Lyubetskaya and Korenaga, 2007; Hu and Gao, 2008; Henrique-Pinto et al., 2016). Abbreviation: BPU = Bedded Pyrrhotite Unit.

Fig. 7. Mantle normalized chalcophile elements recalculated to 100 % sulfides and plotted in order of compatibility with picrite mantle (Barnes, 2016) of A) BPU rocks, norites and gabbronorites and B) massive sulfides. A) Note that the concentrations of the elements from

Co to Se increase from the contact aureole rocks to the norites through the BPU xenoliths with the highest concentrations in gabbronorites. Arsenic and Sb concentrations are the highest in the xenolith-hosted sulfides whereas the other sulfides from the other rocks types contain similar to each other. Lead concentrations are similar in all rock types. B) Note that the massive sulfides contain similar concentrations of Co, Ni, Ir, Ru and Rh to the norite-hosted sulfides but are depleted in most other chalcophile elements. In addition the massive sulfides have negative Pt anomalies. Abbreviation: BPU = Bedded Pyrrhotite Unit.

Fig. 8. Variations of semimetals and PGE contents, A) As, B) Sb, C) Pd and D) Ir in 100% sulfides with distance from contact in the B1-384 borehole, Mesaba deposit.

Contact between Virginia Formation sedimentary rocks and mafic magma corresponds to distance zero. Arsenic, Sb, Pd and Ir values are plotted for rocks in the basal unit of the Partridge River Intrusion, i.e. Unit I. Semimetals contents of sulfides decreases with distance from the Bedded Pyrrhotite Unit xenoliths whereas Pd and Ir contents of the norite and gabbronorite-hosted sulfides increase with distance from xenoliths. Abbreviation: BPU = Bedded Pyrrhotite Unit.

Fig. 9. Plots of Cu vs. A) δ_{34}S isotopic ratio, B) Pd, C) Bi, D) Te, E) As and F) Sb in 100% sulfides of rocks within the intrusion and results of the modeling.

Red line represents interaction model from calculation based on equations of Lesher and Burnham, 2001. Numbers along the line represent different R factor values. Models for As and Sb are plotted for partition coefficients at 900°C and 1000°C. Abbreviation: BPU = Bedded Pyrrhotite Unit.

Fig. 10. Proposed model for S and semimetals contamination of the mafic magma.

A) Partial melting of Bedded Pyrrhotite Unit xenoliths in the magma. Sulfides are transferred to the mafic magma via anatectic silicate melt. This transfer leads to S and semimetals contamination of the mafic magma. In addition, diffusive transfer of Ni, Cu and trace metals from the mafic magma to the Bedded Pyrrhotite Unit xenolith occurs. Low R factor are recorded in the mafic magma. B) Massive sulfide accumulation after increase of partial melting degree. Massive sulfides are PGE-poor because of lack of interaction with the magma. C) Magma disturbance, i.e. new injection of magma or possibly related to seismic fault activity, results in sulfide transportation. Platinum-group element enrichment of sulfide droplets occurs because of high R-factor of the mafic magma. Large-scale sulfur and semimetals contamination of the mafic magma occurs in the basal unit. Hence, platinum-group minerals are present in gabbronorites in the whole basal unit I. Abbreviations: BPU = Bedded Pyrrhotite Unit; PGE = Platinum-group elements.

	As (ppm)	Sb (ppm)	Bi (ppm)	Te (ppm)
BPU average – This study	38	4.1	0.6	0.4
SDO-1 average (Henrique-Pinto et al., 2016)	62.6	4.11	0.27	0.131
SCHS-1 average (Henrique-Pinto et al., 2016)	50.1	0.072	0.102	-
SBC-1 average (Henrique-Pinto et al., 2016)	29.4	1.22	0.6	0.184
SH-1 average (Henrique-Pinto et al., 2016)	22.5	1.17	1.19	0.198
Median black shale (Ketris and Yudovich, 2009)	30	5	1.1	2
Upper crust average (Hu and Gao, 2008)	5.7	0.75	0.23	0.027
MORB average (Arevalo and McDonough, 2010)	0.11	0.014	0.01	0.005
Picrites average (Dionne-Foster, 2007)	0.45	0.02	0.01	0.02
Primitive mantle average (Lyubetskaya and Korenaga, 2007)	0.05	0.007	0.004	0.008

Table 1. Average semimetals contents of the Bedded Pyrrhotite Unit in comparison with average and median values of black shale standards (SDO-1, SCHS-1, SBC-1 and SH-1), black shale, upper crust, MORB, picrites and primitive mantle.

Abbreviations: BPU=Bedded Pyrrhotite Unit; MORB=Mid-oceanic ridge basalt; SDO-1= Devonian Ohio Shale; SCHS-1= Carbonaceous black shale; SBC-1= Brush Creek Shale; SH-1= In-house black shale.

Table 2. Average values of chalcophile elements in the Partridge River Intrusion and the contact aureole rocks, recalculated to 100 % sulfides. Abbreviations: BPU=Bedded Pyrrhotite Unit; c.a.=contact aureole; n.d.=not determined.

	Mo ppm	As ppm	Sb ppm	Pb ppm	Bi ppm	Se ppm	Ag ppm	Cu ppm	Au ppb	Te ppm	Pd ppb	Pt ppb	Rh ppb	Ru ppb	Ir ppb	Os ppb	Ni ppm	Co ppm
BPU c.a. (n=11)	197	273	18	221	3	24	11	1842	40	2	17	43	2	1	0.4	2	1381	217
BPU xenoliths (n=26)	128	540	72	165	8	20	40	16698	669	3	240	149	19	58	4	9	7468	1322
Massive sulfides (n=6)	52	105	1	13	1	40	9	28163	1982	2	960	60	89	54	27	7	18951	2091
Norites (n=32)	288	255	30	275	12	43	41	71849	3119	11	3296	1722	74	97	27	23	22826	2596
Gabbronorites (n=27)	n.d.	147	28	n.d.	7	80	61	128300	12675	12	15906	3729	452	337	80	43	44577	2872

Table 3. Results of modeling of compositions of sulfides.

R Factor:	As (ppm)	As (ppm)	Sb (ppm)	Sb (ppm)	Bi (ppm)	Te (ppm)	Cu (ppm)	Pd (ppb)	δ^{34}S (‰)
0	837.00	837.00	73.00	73.00	3.00	3.00	17621	263.0	13.40
2	832.35	698.25	72.56	60.87	3.01	3.04	17903	278.8	13.37
4	827.76	599.14	72.12	52.20	3.03	3.08	18185	294.5	13.34
10	814.35	420.75	70.84	36.60	3.07	3.19	19026	341.8	13.24
50	736.71	143.25	63.43	12.33	3.33	3.96	24508	656.6	12.63
500	398.25	20.82	31.13	1.63	5.33	11.70	74097	4179.8	8.48
1000	297.00	12.74	21.46	0.92	6.50	18.82	111747	8053.5	6.35
2000	226.57	8.64	14.74	0.56	7.67	29.77	158811	15674.7	4.41
3200	195.17	7.09	11.74	0.43	8.33	39.16	191393	24604.2	3.38
6400	166.43	5.80	9.00	0.31	9.05	54.08	232767	47329.4	2.32
Concentrations in sedimentary sulfides	837	837	73	73	3	3	17621	263	-
Concentrations in silicate magma	0.45	0.45	0.02	0.02	0.01	0.02	150	7.88	-
Dsulfide/silicate	300	10	300	10	1000	4500	2000	90000	-
Temperature (°C)	900	1100	900	1100	-	-	-	-	-
δ^{34}S magma	-	-	-	-	-	-	-	-	1
δ^{34}S sediments	-	-	-	-	-	-	-	-	13.4

Calculations are based on equation 5 in Lesher and Burnham (2001). Grey section corresponds to final concentrations of elements in the sulfide magma after modeling. Values for model calculations are concentrations of elements in the sedimentary sulfides, i.e. average of the BPU xenolith concentrations; concentrations of elements in silicate magma, i.e. average of picrites concentrations (Dionne-Foster, 2007); concentrations of elements in the silicate magma, i.e. average of picrite concentrations (Dionne-Foster, 2007) and partition coefficients between sulfide and silicate melts (Li and Audétat, 2012; Kiseeva and Wood, 2013; Patten et al., 2013; Brenan, 2015; Li and Audétat, 2015; Liu and Brenan, 2015). Abbreviations: BPU=Bedded Pyrrhotite Unit.

Appendix A. Stratigraphic position of the samples in the boreholes sections of Virginia Formation country-rocks and the basal part (Unit I) of the Partridge River Intrusion (modified from Queffurus and Barnes, 2014). The few samples taken from Dunka Pit, A4-15, 26014, 26015, B1-46, B1-129, CN-7 and LE-3 are not indicated.

Abbreviations: PRI = Partridge River intrusion, BPU = Bedded Pyrrhotite Unit

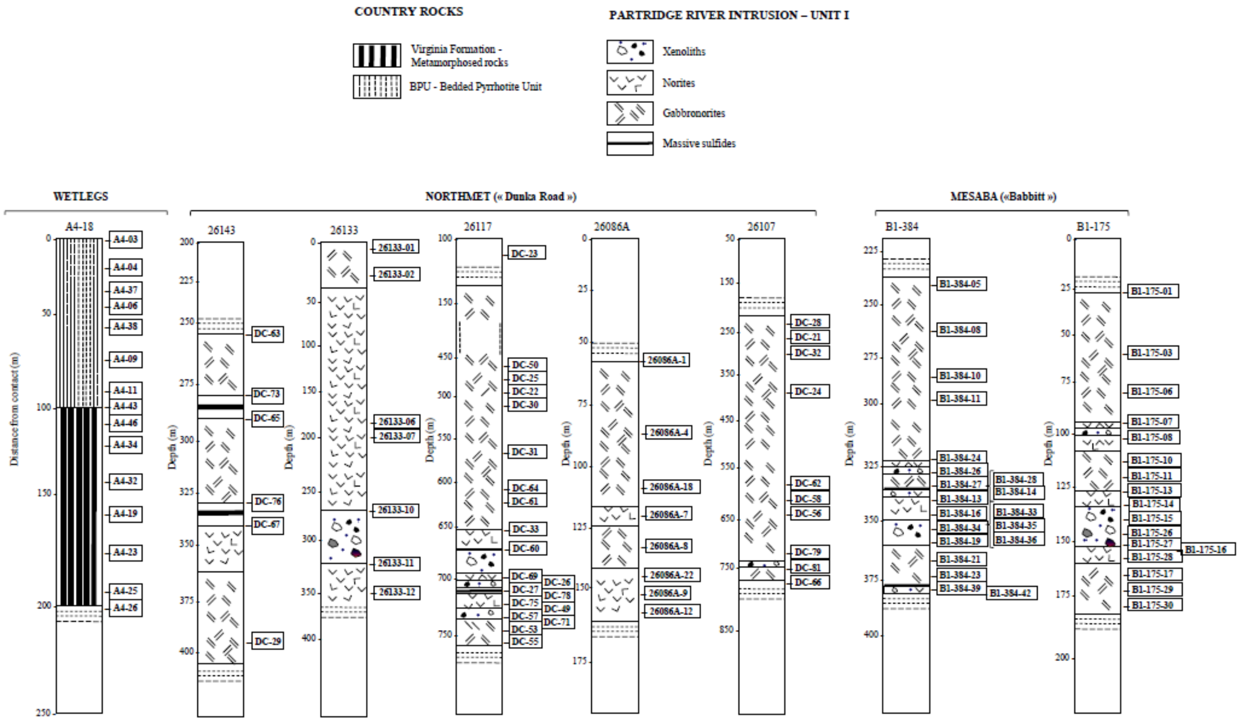

Appendix B1. Whole-rock data for the Bedded Pyrrhotite Unit from the contact aureole. xenoliths of the Bedded Pyrrhotite Unit. norites and gabbronorites. Abbreviations: BPU=Bedded Pyrrhotite Unit; c.a.=contact aureole.

			S and δ34S		**Semimetals**				**Major and trace elements**													
Samples	Rock type	Deposit	S (%)	δ34S (‰ VCDT)	As (ppm)	Sb (ppm)	Bi (ppm)	Te (ppm)	Ni (ppm)	Cu (ppm)	Co (ppm)	Ag (ppm)	Se (ppm)	Pb (ppm)	Mo (ppm)	Os (ppb)	Ir (ppb)	Ru (ppb)	Rh (ppb)	Pt (ppb)	Pd (ppb)	Au (ppb)
DC-70	BPU c.a.	Dunka Pit	4.45	16.3	15.16	1.53	0.28	<0.06	130	140	26	1.10	1.60	24.52	28.00	<1.5	0.1	<5.0	0.1	4.9	0.8	1.7
B1-331-01	BPU c.a.	Mesaba	4.30	-	29.01	0.50	0.52	0.19	120	170	22	1.70	-	20.00	20.72	0.3	-	0.2	0.2	3.1	2.2	2.3
B1-338-01	BPU c.a.	Mesaba	5.60	-	13.76	2.56	0.53	0.08	90	290	25	1.50	-	42.65	30.00	0.3	0.1	0.2	0.2	9.7	1.2	2.7
A4-01	BPU c.a.	Wetlegs	6.53	-	10.00	2.60	0.20	-	187	197	28	2.10	-	37.00	37.00	0.2	0.1	0.2	0.7	9.3	2.4	15.8
A4-03	BPU c.a.	Wetlegs	2.26	-	31.57	1.52	0.24	<0.06	289	313	27	1.29	1.11	12.64	-	-	-	-	-	-	-	-
A4-04	BPU c.a.	Wetlegs	6.30	20.4	22.40	5.85	-	-	140	200	-	-	2.41	-	-	-	-	-	-	-	-	-
A4-	BPU	Wetl	4.	16.	13.	2.2	0.1	-	80	14	22	1.1	3.1	35.0	26.	0.	0.	0.	0.	-	1.8	7.

09	c.a.	egs	19	7	00	0	2			0		0	1	0	00	4	1	2	3			1
A4-11	BPU c.a.	Wetlegs	6.67	18.3	22.86	1.90	0.49	0.55	150	260	34	0.90	4.42	38.00	23.87	<0.2	-	0.1	0.1	6.1	1.2	3.5
A4-12A	BPU c.a.	Wetlegs	5.85	-	27.00	1.90	0.12	-	150	310	29	1.60		27.00	31.00	0.2	0.1	0.2	0.3	6.2	8.0	8.5
A4-38	BPU c.a.	Wetlegs	2.23	19.5	31.40	1.38	-	-	101	130	-	-	2.23	-	-	-	-	-	-	-	-	-
A4-43	BPU c.a.	Wetlegs	1.45	-	35.00	1.17	-	-	67	59	-	-	1.40	-	-	-	-	-	-	-	-	-
EC-07-A	BPU xenolith	Dunka Pit	2.50	-	22.00	3.00	2.20	0.28	730	3965	86	1.40	2.40	15.88	2.75	-	0.3	1.1	1.3	22.7	58.4	26.6
B1-384-14	BPU xenolith	Mesaba	7.13	9.5	47.00	1.05	1.50	0.07	2720	4129	307	1.40	6.15	20.49	25.00	0.3	-	0.2	0.3	15.3	144.8	6.2
B1-384-18	BPU xenolith	Mesaba	7.70	-	63.22	10.47	-	-	2192	4666	218	4.24	-	-	-	<1.2	0.6	<7.3	2.1	4.0	27.4	14.8
B1-384-19	BPU xenolith	Mesaba	5.48	11.5	112.42	4.88	0.45	0.64	607	1986	54	7.45	2.45	37.39	-	0.4	0.1	3.3	<0.1	0.9	12.5	11.1
B1-384-207	BPU xenolith	Mesaba	1.24	-	24.95	6.30	-	-	457	981	48	-	-	-	-	0.2	-	2.9	<2.2	1.4	<9.1	24.2
B1-	BPU	Mesa	3.	18.	22.	0.4	0.4	0.2	90	31	15	1.0	3.7	19.0	24.	<0	0.	2.	1.	9.	41.	16

384-26	xenolith	ba	74	1	00	0	0	6	0	00	2	0	1	1	28	.6	2	6	0	3	7	.2
B1-384-33	BPU xenolith	Mesaba	5.33	10.7	36.42	2.70	0.70	0.45	1120	3371	129	2.40	2.25	44.00	20.44	0.3	-	0.2	-	1.4	11.5	4.3
B1-384-34	BPU xenolith	Mesaba	5.22	11.7	48.00	2.42	0.50	0.63	535	1221	32	5.94	2.73	29.68		0.2	-	2.8	0.2	51.4	3.9	2.0
B1-384-35	BPU xenolith	Mesaba	6.38	12.2	40.12	2.80	1.00	0.46	430	1926	73	1.30	2.43	31.00	24.56	0.3	-	-	-	0.7	3.5	2.9
B1-384-36	BPU xenolith	Mesaba	6.36	14.2	23.00	2.80	0.80	0.26	410	2067	60	1.30	2.84	17.85	18.50	0.3	-	0.2	0.1	1.7	9.6	6.3
B1-46-02	BPU xenolith	Mesaba	0.47	-	35.51	6.24	-	-	125	144	18	1.44	-	-	-	<0.2	-	<2.7	<0.2	2.9	2.7	4.9
B1-46-05a	BPU xenolith	Mesaba	2.72	-	34.15	8.88	-	-	264	438	23	1.73	1.43	-	-	0.6	-	2.5	0.2	1.7	3.5	2.9
B1-46-11	BPU xenolith	Mesaba	4.55	-	-	-	-	-	-	-	-	-	2.19	-	-	-	-	-	-	-	-	-
26014-01a	BPU xenolith	North Met	1.24	-	18.58	4.84	-	-	195	251	46	-	1.15	-	-	<.35	0.1	4.0	0.5	2.2	2.6	6.0
2608	BPU	North	3.	-	36.	2.3	-	-	97	11	82	2.3	-	-	-	<0	0.	5.	4.	<1	93.	2.

6A-11	xenolith	Met	81		42	3			3	23		1				.2	6	3	5	.6	9	7
DC-26	BPU xenolith	North Met	0.70	-	14.43	1.06	-	-	150	422	166	-	-	-	-	0.7	0.3	<2.9	0.7	6.0	2.9	144
DC-69	BPU xenolith	North Met	5.90	16.9	65.20	<0.2	<0.1	0.48	670	930	157	0.50	1.91	0.15	28.43	1.2	0.8	7.5	1.4	13.1	36.1	282
DC-71	BPU xenolith	North Met	10.20	15.9	9.00	0.50	<0.1	-	280	1060	44	-	0.13	19.00	11.00	<0.6	0.3	0.3	1.3	3.6	40.7	43.0
DC-78	BPU xenolith	North Met	1.56	-	5.99	0.20	-	-	355	732	69	-	-	-	-	0.7	0.2	1.7	0.4	9.0	5.3	122
DC-81	BPU xenolith	North Met	0.40	-	82.90	1.07	-	-	291	420	83	-	-	-	-	0.6	0.3	<2.6	0.3	7.4	8.3	72
B1-175-08	BPU xenolith	Serpentine	1.29	-	11.41	4.23	-	-	414	662	67	8.72	0.78	-	-	0.5	0.5	8.5	1.5	9.0	11.2	4.8
B1-175-15	BPU xenolith	Serpentine	4.53	-	178.87	9.46	-	-	867	1928	70	5.25	1.62	-	-	0.4	0.1	3.9	0.4	4.8	17.9	13.6
B1-175-26	BPU xenolith	Serpentine	4.88	-	50.58	8.28	-	-	697	1590	55	4.56	1.05	-	-	0.3	0.1	1.9	8.8	0.9	8.2	6.9
B1-17	BPU xen	Serpenti	5.4	-	73.3	5.48	-	-	108	219	133	0.89	1.42	-	-	0.3	0.1	10.	0.2	2.6	23.0	9.4

5-27	olith	ne	8		6				6	6								1				
26133-11	BPU xenolith	Wyman creek	1.19	-	22.19	1.25	-	-	366	202	66	-	-	-	-	-	0.2	8.6	1.8	33.4	8.7	13.4
B1-384-28	Massive sulfides	Mesaba	19.75	12.0	-	-	-	-	-	-	-	-	21.44	-	-	-	-	-	-	-	-	-
B1-384-39	Massive sulfides	Mesaba	16.30	12.3	43.97	0.08	0.17	2.57	9890	30108	960	6.80	24.51	5.79	23.00	8.5	8.0	39.5	14.9	5.4	63.1	22.1
DC-73	Massive sulfides	North Met	19.64	8.4	33.27	0.19	0.60	0.42	10691	12154	1097	1.10	25.00	-	-	1.2	38.2	26.9	116.4	88.9	469.9	286
DC-74	Massive sulfides	North Met	22.20	-	25.22	0.37	1.80	0.52	14518	18206	1586	1.96	22.00	-	-	3.5	9.3	18.9	32.0	32.5	626.5	3471
DC-75	Massive sulfides	North Met	31.20	16.0	174.79	0.39	0.59	1.07	6840	11369	1245	11.50	13.00	-	-	3.8	2.3	<9.3	11.8	23.2	876.7	1310
DC-76	Massive sulfides	North Met	34.90	12.0	104.39	2.39	1.36	0.85	18731	5423	-	-	43.00	-	-	4.6	27.0	39.9	116.9	34.6	1590.0	<2
B1-384-04a	norite	Mesaba	0.03	-	<5	<0.2	<0.1	<0.06	260	950	18	-	1.47	7.00	2.00	0.8	0.6	2.5	1.2	9.0	10.9	1.2
B1-38	norite	Mesaba	1.2	-	22.0	0.50	<0.1	<0.0	157	650	134	1.00	3.08	17.00	<2	0.6	0.9	4.7	2.1	22.	47.9	15.

4-12			7		0			6	0	0										7		5
B1-384-13	norite	Mesaba	1.72	13.2	8.20	1.20	-	-	786	2164	108	2.27	1.87	-	-	<0.4	0.3	4.4	0.9	10.3	27.1	12.8
B1-384-15	norite	Mesaba	1.58	-	8.45	1.65	-	-	1100	4862	125	2.26	-	-	-	<0.4	0.7	3.4	1.8	23.5	52.4	27.5
B1-384-16	norite	Mesaba	7.17	12.5	29.00	<0.2	0.20	-	470	1830	81	0.50	2.98	8.00	<2	0.7	2.1	5.1	4.3	9.3	36.8	33.3
B1-384-24	norite	Mesaba	3.17	-	9.12	1.91	-	-	976	2280	144	0.66	4.11	-	-	0.8	1.3	5.2	2.9	13.6	43.1	18.7
B1-384-27	norite	Mesaba	2.31	-	21.49	0.86	-	-	2179	2974	172	3.72	-	-	-	<1.4	2.5	7.5	7.0	105.5	1132.2	480
B1-384-30	norite	Mesaba	2.29	-	9.09	1.64	-	-	1240	4336	134	2.44	-	-	-	0.6	0.7	2.3	1.9	25.2	64.3	23.9
B1-384-42	norite	Mesaba	6.31	12.2	6.52	0.17	0.11	1.07	3513	11649	257	3.90	-	-	-	2.9	2.3	12.1	5.1	1.9	92.0	22.1
26086A-05	norite	NorthMet	2.80	-	28.08	1.88	-	-	1269	4887	135	7.33	-	-	-	0.7	1.5	3.7	14.6	53.0	340.3	76.6
26086A-	norite	NorthMet	3.61	-	51.18	2.23	-	-	1200	3131	101	2.23	-	-	-	1.0	0.3	9.7	1.5	13.3	94.2	48.2

06.																						
26086A-07	norite	NorthMet	1.62	-	14.30	1.69	-	-	1031	3615	112	4.39	2.04	-	-	1.0	1.3	4.9	<0.5	141.8	282.3	48.2
26086A-09	norite	NorthMet	1.51	-	21.24	3.18	-	-	724	1615	85	1.65	1.33	-	-	<0.8	0.8	2.1	3.5	180.6	143.3	17.7
26086A-10	norite	NorthMet	5.49	-	33.07	2.50	-	-	2264	6020	252	2.10	-	-	-	2.7	9.7	7.8	16.3	245.4	2126.4	31.9
26086A-12	norite	NorthMet	0.91	-	3.79	2.41	-	-	560	2499	74	2.40	1.66	-	-	<0.5	0.6	4.2	3.1	38.6	151.2	30.8
26086A-22	norite	NorthMet	3.36	-	41.00	1.97	-	-	1212	3438	149	2.69	2.58	-	-	<0.5	1.0	5.2	4.4	35.2	171.7	29.3
DC-27	norite	NorthMet	0.77	14.5	10.00	<0.2	0.11	-	330	860	101	0.70	0.92	6.00	6.00	<0.6	0.3	<2.6	0.9	12.8	22.7	-
DC-49	norite	NorthMet	0.20	8.2	1.96	1.59	-	-	151	373	52	-	-	-	-	<0.5	0.1	<5.0	<0.2	2.5	5.4	<2
DC-52	norite	NorthMet	0.66	13.7	6.28	1.35	-	-	186	293	40	-	-	-	-	<0.9	0.3	4.9	0.7	3.7	11.1	<2
DC-54	norite	NorthMet	0.31	12.5	2.77	0.80	-	-	265	622	62	-	-	-	-	0.7	0.2	<5.0	0.6	6.9	8.1	23
DC-57	norite	NorthM	1.4	-	28.9	2.47	-	-	188	814	96	3.88	-	-	-	2.5	7.6	7.7	16.	554	423.	309

		et	9		6				5	0									9	.5	5	
DC-60	norite	NorthMet	1.57	10.4	3.42	0.57	-	-	1140	3000	127	0.75	-	-	-	<1.3	1.2	<5.0	4.8	50.2	104.7	185
DC-67	norite	NorthMet	3.42	5.3	6.89	0.62	5.19	2.10	1570	13996	138	2.03	-	-	-	4.1	2.0	5.3	7.1	835.3	974.2	2763
DC-68	norite	NorthMet	3.39	-	2.11	0.10	0.82	0.42	1553	14052	137	2.48	-	-	-	2.9	1.7	<5.3	7.2	642.4	932.3	2133
B1-175-03	norite	Serpentine	3.98	-	17.52	3.53	-	-	1680	5424	179	4.21	4.15	-	-	0.5	0.9	6.9	2.0	26.0	100.3	47.1
B1-175-07	norite	Serpentine	7.08	10.6	13.78	0.25	0.46	2.34	3037	5397	344	2.56	5.77	-	-	0.8	1.5	3.5	2.0	6.7	84.3	23.9
B1-175-09	norite	Serpentine	8.35	-	26.53	0.49	-	-	3768	5491	404	2.69	4.87	-	-	2.5	2.3	4.1	4.7	10.6	59.1	45.1
B1-175-10	norite	Serpentine	3.17	-	15.33	1.51	-	-	1867	5450	170	3.71	5.01	-	-	0.7	1.2	3.5	3.5	38.8	88.1	90.2
B1-175-13	norite	Serpentine	4.78	-	14.58	1.64	-	-	1511	2471	233	-	5.03	-	-	1.8	1.1	5.8	2.3	16.2	49.4	19.3
B1-175-14	norite	Serpentine	2.40	15.3	10.70	2.57	-	-	1114	1226	177	-	2.14	-	-	0.3	0.3	<3.9	0.9	2.6	13.8	7.6

B1-1755-28	norite	Serpentine	0.68	-	6.35	1.63	-	-	364	537	81	-	1.08	-	-	0.5	0.2	2.3	0.5	2.3	7.1	<1.0
CN-7-3	norite	Water-hen	0.27	-	4.61	0.25	-	-	497	673	115	-	-	-	-	1.4	0.1	9.4	0.6	10.5	5.9	3.8
CN-7-6	norite	Water-hen	1.80	-	25.06	0.21	-	-	1002	1121	142	1.35	-	-	-	-	-	-	-	-	-	-
26133-06	norite	Wymancreek	1.29	-	0.65	0.07	-	-	2071	6525	112	2.99	-	-	-	0.9	3.4	4.3	4.3	43.2	8.7	16.9
26133-07	norite	Wymancreek	0.81	-	0.90	0.05	-	-	1462	3828	139	0.43	-	-	-	1.4	1.3	7.8	4.1	56.7	11.1	44.2
26133-10	norite	Wymancreek	0.14	-	2.92	0.19	-	-	703	630	144	-	-	-	-	1.7	1.0	5.4	3.3	378.8	38.7	4.2
26133-12	norite	Wymancreek	0.11	-	0.86	0.12	-	-	279	309	62	-	-	-	-	1.3	0.8	7.1	1.8	18.2	1.7	1.2
LE-3-01	Gabbronorite	Longear	0.02	-	0.19	0.04	-	-	430	48	61	-	-	-	-	1.1	0.1	6.7	0.6	7.8	3.8	0.4
B1-384-05	Gabbronorite	Mesaba	1.77	12.0	<5	<0.2	<0.1	<0.06	650	760	129	-	0.42	<5	<2	2.7	4.1	17.9	19.3	109.4	426.9	192.1
B1-	Gabbr	Mesa	1.	6.1	1.8	0.0	0.7	1.3	18	77	11	3.8	10.	<5	-	2.	10	22	39	42	13	16

384-08	onorite	ba	80		6	9	7	6	04	18	6	6	91			0	.0	.5	.3	2.5	93.4	.9
B1-384-10	Gabbronorite	Mesaba	4.04	7.7	0.72	0.94	-	-	2337	27472	96	14.98	-	-	-	1.8	2.4	13.8	1.7	58.6	296.1	119.2
B1-384-11	Gabbronorite	Mesaba	1.91	-	5.83	0.87	-	-	4524	5767	230	4.42	-	-	-	1.8	3.1	13.5	14.2	59.7	510.6	26.9
B1-384-21	Gabbronorite	Mesaba	0.29	12.4	<5	<0.2	<0.1	<0.006	390	2070	87	-	0.72	7.00	<2	<0.5	0.2	<2.1	0.3	5.1	16.5	7.5
B1-384-23	Gabbronorite	Mesaba	2.81	-	4.39	1.20	-	-	1556	10153	131	4.70	-	-	-	0.6	0.8	5.1	1.7	168.3	39	12.1
26086A-01	Gabbronorite	North Met	0.09	-	1.03	1.91	-	-	312	512	53	-	0.50	-	-	0.3	0.6	2.1	1.9	24.8	88.5	7.2
26086A-03	Gabbronorite	North Met	1.25	-	1.42	1.06	-	-	3075	5834	97	3.89	-	-	-	2.0	6.4	8.6	29.8	443.0	1085.3	939
26086A-04	Gabbronorite	North Met	1.25	-	1.09	0.72	-	-	7379	3065	188	1.43	3.33	-	-	1.8	3.3	15.8	29.5	71.6	2083.1	57.9
26086A-08	Gabbronorite	North Met	0.82	-	1.27	0.89	-	-	1233	4386	80	3.23	2.80	-	-	0.9	3.3	9.2	19.2	176.1	961.4	291.9
26086	Gabbrono	North M	0.4	10.7	3.48	1.97	-	-	520	772	58	0.72	0.71	-	-	1.1	0.4	10.	2.2	9.9	42.8	5.4

A-18	rite	et	5															8				
26086A-21	Gabbronorite	NorthMet	5.01	12.8	21.68	0.78	-	-	3382	5231	272	2.88	-	-	-	0.2	3.3	<14	14.7	54.3	315.6	129.6
DC-21	Gabbronorite	NorthMet	0.25	-	<0.33	0.34	-	-	228	112	76	-	-	-	-	<0.9	0.2	<8.2	0.2	4.5	4.5	-
DC-22	Gabbronorite	NorthMet	0.01	-	<0.33	0.47	-	-	295	169	84	-	-	-	-	<0.5	0.0	<5.4	<0.2	<2.4	<2.8	2
DC-23	Gabbronorite	NorthMet	0.01	-	<5	<0.2	<0.1	<0.06	310	270	66	-	0.16	<5	<2	<1.3	0.3	4.9	0.8	6.7	10.6	32
DC-24	Gabbronorite	NorthMet	0.06	-	0.86	1.62	-	-	189	164	74	-	-	-	-	1.1	0.1	<2.7	0.2	3.1	3.7	48
DC-25	Gabbronorite	NorthMet	<.01	-	0.34	0.31	-	-	198	129	62	-	-	-	<2	0.4	0.3	<2.0	0.5	<5.3	6.1	31
DC-28	Gabbronorite	NorthMet	0.01	-	<0.39	0.45	-	-	266	62	74	-	-	-	-	<1.3	0.4	<3.1	0.1	<5.1	<2.8	19
DC-29	Gabbronorite	NorthMet	0.03	-	0.82	4.35	-	-	123	155	44	-	-	-	-	<0.6	0.4	<2.5	0.4	8.5	6.9	59
DC-30	Gabbronorite	NorthMet	<.01	-	<5	<0.2	<0.1	<0.06	150	30	36	-	0.02	<5	-	<0.7	0.3	<3.3	1.5	<6.0	17.0	421
DC-31	Gabbronorite	NorthMet	<.01	-	<0.44	0.64	-	-	97	87	62	-	-	-	-	0.5	0.1	<5.0	0.9	9.6	2.0	18
DC-32	Gabbrono	NorthM	0.0	-	<0.5	1.07	-	-	244	132	69	-	-	-	-	<0.	0.1	<1.	0.4	5.5	3.3	89

	rite	et	3		0											9		7				
DC-33	Gabbronorite	NorthMet	0.06	-	<0.43	0.50	-	-	190	173	97	-	-	-	-	<0.8	0.1	<4.1	0.3	<4.7	3.1	265
DC-50	Gabbronorite	NorthMet	0.09	-	<5	<0.2	<0.1	<0.06	180	450	60	-	0.18	<5	<2	<1.2	0.3	<2.2	0.5	7.4	14.2	<2
DC-53	Gabbronorite	NorthMet	0.15	6.7	2.23	1.03	-	-	230	514	55	-	-	-	-	<0.8	0.6	<5.0	1.5	10.2	39.0	-
DC-55	Gabbronorite	NorthMet	1.11	9.0	2.73	0.14	0.23	0.45	1073	3652	89	0.28	-	-	-	0.9	1.0	6.9	5.1	42.1	174.3	322
DC-56	Gabbronorite	NorthMet	1.44	9.2	3.52	2.86	-	-	1909	5550	170	1.37	-	-	-	1.6	2.8	12.9	14.4	111.7	402.1	476
DC-58	Gabbronorite	NorthMet	2.00	6.6	0.71	2.65	-	-	2439	10228	113	0.79	-	-	-	1.9	3.0	10.3	19.3	160.7	712.2	1440
DC-59	Gabbronorite	NorthMet	0.12	-	0.34	1.10	-	-	567	1014	68	-	-	-	-	<1.4	0.1	<3.1	0.3	<5.4	5.1	-
DC-61	Gabbronorite	NorthMet	1.50	7.5	<0.38	0.56	-	-	2051	7129	113	1.23	-	-	-	2.5	3.8	16.2	18.2	124.3	501.3	589
DC-62	Gabbronorite	NorthMet	1.69	1.6	2.68	0.14	0.22	0.30	3742	12249	150	1.55	-	-	-	3.2	10.5	34.2	79.9	559.7	2250.6	4214
DC-63	Gabbronorite	NorthMet	2.45	7.1	7.53	0.14	0.36	0.38	824	2210	180	0.48	-	-	-	1.2	0.9	<5.0	3.2	15.6	62.9	184
D	Ga	No	0	2.	<	<	<	<	6	6	7	-	3.	<	<	4	8	3	5	2	1	8

C-64	bbronorite	rthMet	.59	8	5	0.2	0.1	0.06	40	90	5		30	5	2	.1	.6	1.5	8.0	99.1	630.4	87
DC-65	Gabbronorite	NorthMet	2.17	11.9	14.83	1.38	-	-	1465	15662	109	3.91	-	-	-	2.3	0.4	<5.0	2.9	371.1	600.7	2650
DC-66	Gabbronorite	NorthMet	4.32	9.8	22.58	0.35	0.69	0.77	2283	6395	310	1.02	-	-	-	2.2	4.3	20.3	23.0	35.1	463.7	451
DC-79	Gabbronorite	NorthMet	1.12	7.6	4.68	0.60	-	-	2246	7120	120	-	-	-	-	1.3	3.0	10.1	15.0	163.9	583	667
B1-175-01.	Gabbronorite	Serpentine	3.21	-	12.36	1.58	-	-	2506	8240	198	6.33	5.48	-	-	<0.9	1.5	4.6	3.4	18.4	133	45.7
B1-175-06	Gabbronorite	Serpentine	0.92	13.7	20.84	2.44	-	-	783	2719	89	3.18	1.25	-	-	<0.7	0.4	3.1	1.7	17.4	60.0	20.4
B1-175-11	Gabbronorite	Serpentine	2.02	-	17.86	2.04	-	-	1017	5362	127	4.33	2.63	-	-	0.6	0.8	1.9	1.7	85.6	65.8	20.9
B1-175-16	Gabbronorite	Serpentine	6.52	-	35.13	0.58	-	-	1194	4190	173	2.01	2.14	-	-	2.3	1.0	10.0	2.5	<1.4	39.2	35.9
B1-175-17	Gabbronorite	Serpentine	4.58	-	3.73	2.21	-	-	2541	9797	225	3.31	5.22	-	-	0.9	1.4	2.8	2.4	21.8	55.8	20
B1-	Gabbr	Serpe	2.	-	11.	2.0	-	-	14	14	11	9.2	3.2	-	-	0.	1.	4.	2.	70	91.	36

175-29	onorite	ntine	33		70	2			27	283	5	2	9			8	0	0	5	.4	8	.7
B1-175-30	Gabbronorite	Serpentine	3.00	15.2	3.31	0.16	0.34	0.86	2257	5318	193	3.21	3.92	-	-	0.5	1.0	2.5	2.4	25.5	68.7	25.2
26133-01	Gabbronorite	Wyman creek	0.04	-	0.30	0.05	-	-	205	51	43	-	-	-	-	0.8	0.1	7.1	1.4	7.0	0.5	0.5
26133-02	Gabbronorite	Wyman creek	0.03	-	0.39	0.07	-	-	236	43	48	-	-	-	-	-	0.1	0.5	0.8	4.3	0.4	0.3

Appendix B2. Values obtained for reference materials.

LabMaTer S determination by infrared spectrometry S-C analyser	S (%)								
KPT-1 this work	1.08								
KPT-1 (Webb et al. 2006)	*1.029+/-.034*								
University of Waterloo Whole-rock δ34S	δ34S (‰ VCDT)								
DC-64 (This study)	3.0								
DC-64 (Duplicate this study)	2.8								
DC-64 (Thériault and Barnes, 1998)	2.5								
B1-384-26 (This study)	18.4								
B1-384-26 (Duplicate this study)	18.6								
B1-384-26 (Queffurus and Barnes, 2014)	17.3								
LabMaTer Semimetals determined by black shale method	As (ppm)	Sb (ppm)	Bi (ppm)	Te (ppm)					
SDO-1 this	68.41	4.69	0.37	0.29					

study									
SDO-1 (Henrique-Pinto et al., 2016)	*62.6+/-1.7*	*4.11+/-0.09*	*0.27+/-0.01*	*0.131+/-0.02*					
SBC-1 this study	34.19	1.19	0.77	0.28					
SBC-1 (Henrique-Pinto et al., 2016)	*29.4+/-1.8*	*1.22+/-0.26*	*0.6+/-0.01*	*0.184+/-0.04*					
SCHS-1 this study	56.19	0.1	0.13	0.07					
SCHS-1 (Henrique-Pinto et al., 2016)	*50.1+/-0.4*	*0.072+/-0.001*	*0.102+/-0.002*	-					
SH-1 this study	27.91	1.54	1.45	0.25					
SH-1 (UQAC)	*22.5+/-2.2*	*1.17+/-0.03*	*1.19+/-0.03*	*0.198+/-0.014*					
KPT-1	2.57	8.49	0.45	0.48					
KPT-1 (Webb et al., 2006)	*2.2+/-0.53*	*10.01+/-1.13*	*0.95+/-0.153*	*0.35+/-0.090*					
WMS-1a	24.39	5.31	0.73	3.28					
WMS-1a (Certificate values CANMET)	*30.9+/-4.8*	*6.29+/-0.98*	*1.2*	*3.7 +/-0.64*					
LabMaTer Selenium determination by TCF-INAA	Se (ppm)								
MRG-1	0.24								
MRG-1(Savard et al., 2009)	*0.199+/-0.008*								
ACTLAB Fusion followed by ICP-MS	Ni (ppm)	Cu (ppm)	Co (ppm)	Ag (ppm)	As (ppm)	Sb (ppm)	Bi (ppm)	Pb (ppm)	Mo (ppm)
KPT-1this study	880	950	83	1.4	7	9.7	0.8	68	2
KPT-1	*1093+/*	*1112+/*	*78.92+*	*0.75+/-*	*2.2+/-*	*10+/-*	*0.95+/*	*81.07+*	*1.72+*

(Webb et al., 2006)	*-71*	*-102*	*/-5*	*0.15*	*0.53*	*1.13*	*-0.15*	*/-0.994*	*/-0.118*
LabMaTer Ni-FA-ICP-MS	Os (ppb)	Ir (ppb)	Ru (ppb)	Rh (ppb)	Pt(ppb)	Pd (ppb)	Au (ppb)		
OKUM - this study	0.7	0.9	4.5	1.4	10.4	12.0	1.0		
OKUM (Savard et al., 2010)	*0.98+/-0.34*	*0.99 +/-0.07*	*4.25+/-0.3*	*1.40 +/-0.13*	*11+/-0.6*	*11.7+/-0.5*	*1.4*		
SLg-1 black shale - this study FA	<0.16	0.05	0.38	0.52	3.85	1.37	1760		
SLg-1 black shale - this study ID	<0.03	0.06	0.66	-	3.06	0.98	-		
SLg-1 (Li et al., 1998)	*n.d.*	*0.02+/-0.013*	*0.27+/-0.03*	*0.32+/-0.05*	*1.39+/-0.12*	*1.49+/-0.13*	*1690+/-900*		
SLg-1 (Petrov et al., 2004)	*n.d.*	*n.d.*	*1+/-0.4*	*-*	*2.2+/-0.5*	*2.3+/-0.6*	*2500+/-300*		

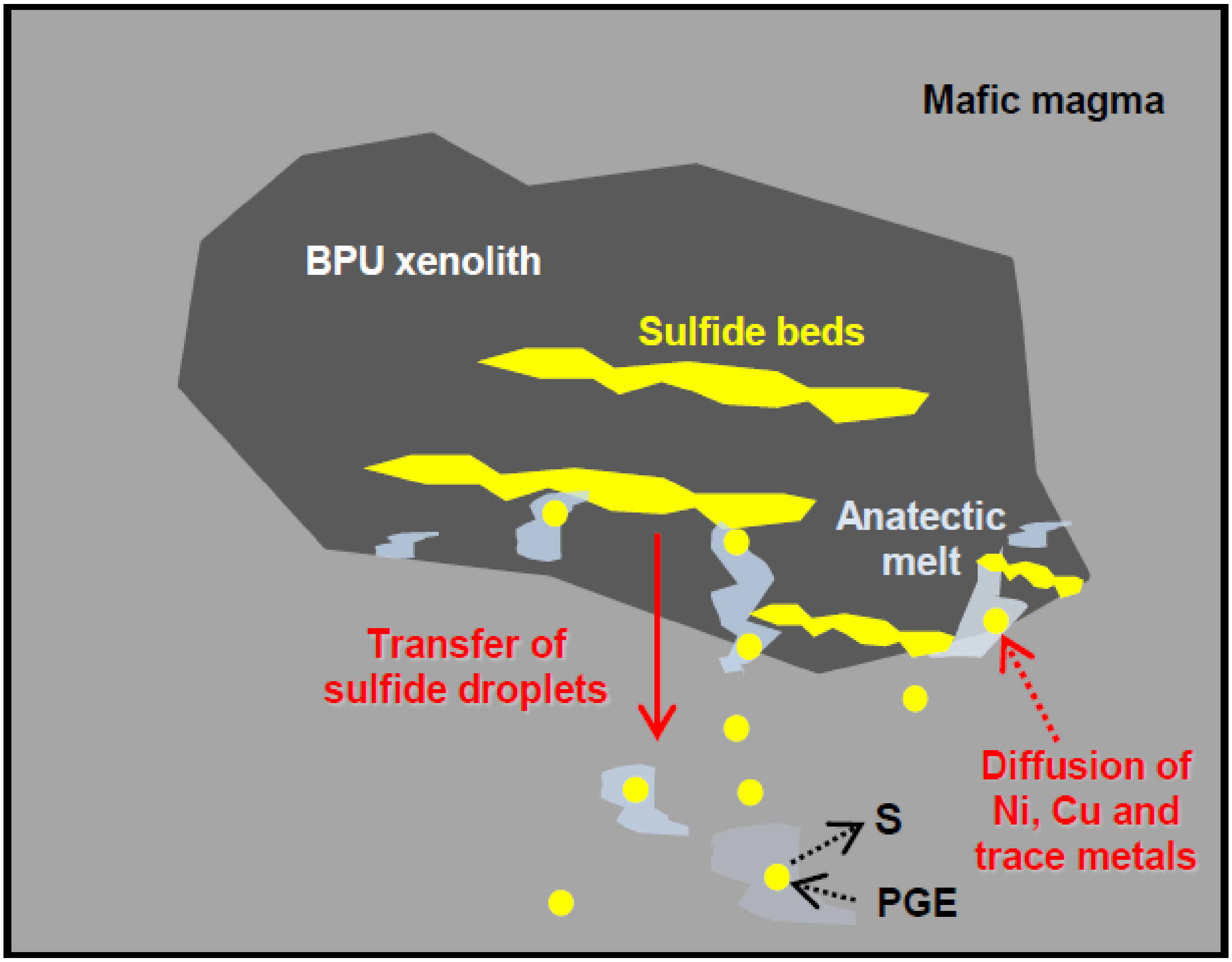

Graphical abstract

Highlights

- We examine interactions between black shale xenoliths and mafic magma.
- Sulfide droplets are entrained in the xenolith melt and transferred to the magma.
- Sulfur and semimetals contamination of the mafic magma is shown and modeled.